2023

A COMPARATIVE ANALYSIS OF COASTDOWN TESTING METHODS FROM AN ELECTRIC DRIVE UNIT ENGAGEMENT PERSPECTIVE USING A STUDENT-DESIGNED PARALLEL HYBRID ELECTRIC VEHICLE

Dawson Everett Dunnuck
West Virginia University, ded00008@mix.wvu.edu

A COMPARATIVE ANALYSIS OF COASTDOWN TESTING METHODS FROM AN ELECTRIC DRIVE UNIT ENGAGEMENT PERSPECTIVE USING A STUDENT-DESIGNED PARALLEL HYBRID ELECTRIC VEHICLE

Dawson Dunnuck

Thesis submitted to the Statler College of Engineering and Mineral Resources at West Virginia University in Partial fulfillment of the requirements for the degree of

Master of Science

In

Mechanical Engineering

Andrew C. Nix Ph.D., Committee Chairperson

Scott Wayne, Ph.D.

Brian Woerner, Ph.D.

Department of Mechanical and Aerospace Engineering Morgantown,

West Virginia

2023

Keywords: Coastdown, Road Load, Hybrid Electric Vehicle, Electric Drive Unit, Road Load Coefficients

Abstract

A COMPARATIVE ANALYSIS OF COASTDOWN TESTING METHODS FROM AN ELECTRIC DRIVE UNIT ENGAGEMENT PERSPECTIVE USING A STUDENT-DESIGNED PARALLEL HYBRID ELECTRIC VEHICLE

Dawson Dunnuck

Coastdown testing and road load determination are pivotal parts of the automotive design process. Vehicle manufacturers and independent companies perform and analyze road loads determined through a coastdown or similar method to determine a vehicle's road load for modeling and EPA certification. For a traditional coastdown, the vehicle's drivetrain must be disconnected through a clutch between the engine and the transmission while traveling at a high rate of speed to place the vehicle in neutral. This changes for hybrid and electric vehicles. Some hybrid, and most electric, vehicles delivered to customers do not have this clutch action to grant the luxury of a traditional neutral. In fact, when coasting, most hybrid or electric vehicles, the electric drivetrain is charging the battery through regenerative braking with negative torque commands. Vehicle manufacturers can successfully disconnect the electric motors and drive units to perform a traditional coastdown with no negative torque. This disconnection is important to isolate the rolling resistance and air resistance without need to account for losses in the electric drive unit. This research aims to test and analyze hybrid and electric vehicle coastdowns where this disconnect is not possible/provided by the manufacturer. The conditions tested enable a hybrid or electric vehicle to coast as intended from the factory with the negative torque through the electric drive unit to recapture energy. The goal of this research is to provide methodology and results to justify testing a hybrid or electric vehicle with its electric drive unit clutch engaged. The testing for this thesis was performed on a 2019 Chevrolet Blazer that West Virginia University's EcoCAR team converted into a P4 parallel hybrid electric vehicle with an internal combustion engine on the front axle and an electric drive unit on the rear. This vehicle's electric drive unit has a clutch that can be disconnected through the team-implemented controls system. To test two post-processing methods to account for the forces of the drive unit outlined by an independent testing organization, the vehicle was subjected to 4 different coastdown conditions. The first condition was a traditional coastdown with the transmission from the engine to the front axle in neutral (all conditions had the transmission in neutral) and the electric drive unit disconnected. The second condition had the electric drive unit engaged with no torque commanded. The last two conditions were the regenerative braking conditions with a "low" torque condition of -200 Nm and the other was a "high" torque condition of -400 Nm. The two regenerative braking condition results were adjusted through two post-processing methods to account for the forces of the drive unit. The second coastdown condition is not statistically the same as the traditional coastdown condition at low vehicle speeds and served as the control for the final two. There all small differences between the two results but none that exceed one standard deviation of the control. Only one post-processing method was viable for the lower regenerative braking torque condition and the calculated road load matches the control. For the higher regenerative braking torque condition, the methods match the road load at vehicle velocities above 15 m/s. Below this velocity, they failed to match the control's road load.

Acknowledgments

I would first like to thank Dr. Andrew Nix for both his influential role as the lead faculty adviser for WVU's EcoCAR team and for his role in my research as my faculty adviser and committee chairperson. When I approached Dr. Nix to come to West Virginia University I was finishing up my bachelor's degree at Rose-Hulman Institute of Technology and I wasn't sure where I wanted to go to complete my master's. Dr. Nix was very inviting and immediately offered for my fiancé (wife now) and I to come out and visit to get a good feel for the program before I committed. He was the only professor I reached out to that both offered and followed through with that level of commitment for a student who had not decided which program to attend. Dr. Nix was also the driving factor to secure my testing time at the Transportation Research Center to perform my testing. He handled all of the communication, legal, and funding aspects of the deal so I could focus on the testing methodology and develop my plans for the day of testing.

Secondly, I would like to thank Dr. Brian Woerner for his role as the CAV and DEI faculty advisor for the WVU EcoCAR team. In between discussing how well IU's and Purdue's basketball teams were this year, Dr. Woerner provided substantial support for the team during my time with it. Dr. Woerner always popped his head into the lab to see where we were with our tasks and made sure that we maintained our focus on the deliverables and our tasks.

I'd like to also thank Dr. Scott Wayne for his role early on in my master's at WVU. Dr. Wayne teaches a hybrid electric vehicle modeling course that was pivotal to my transition into the EcoCAR team's propulsion and controls modeling lead. Without his course and his guidance I would have really struggled to hit the ground running with the team.

Next, I would like to thank my fellow graduate students from both of my years as a team lead. Firstly I would like to thank Jared Diethorn. Jared was very knowledgeable in the field of vehicle modeling as

well as testing best practices. His leadership and guidance is very influential to the growth of the propulsion controls and modeling team. Next, I would like to thank Zachary Flanigan who is the connected and automated vehicle lead. Zach is one of the best managers I have ever met and his dedication to always improving his sensor fusion algorithm has benefited the team tenfold. He also makes a killer playlist. The next person I would like to thank is the engineering manager Colin Kellett. Colin and I worked closely during the architecture selection process for the first year of the EV Challenge and it was clear that our success would have not been possible without him and his team's dedication to EcoCAR. When discussing the team, it is hard to leave out Kaycee Kiser and Morgan Bartley our communications manager and diversity equity and inclusion manager. Kaycee and Morgan navigated the team's outreach and voice to the community with an intensity that can not be matched. They both attribute to the success of this team and the future STEM student across West Virginia. Lastly, I would like to thank David Burley. David is a pivotal member of the team whose knowledge spans many different disciplines. His ability to quickly provide my team with the CAD space claim information was pivotal to our quick simulation of an architecture to input the results into our pugh decision matrix. I would also like to thank Juan Pablo Ibanez for stepping up to the role of project manager and leading us through a difficult information management first year of the EcoCAR EV Challenge.

The final person I would like to acknowledge is Dr. William Cawthorne. Bill goes above and beyond in his role as the EcoCAR GM mentor for the West Virginia team. The role of a mentor is unpaid and voluntary for GM employees. Bill would review every major team deliverable and provide input that was unparalleled. If Bill did not know the answer (which was rare) he would immediately find someone at GM who could provide the answer for our team. Bill and I spent many meetings discussing leadership methodologies and how to deal with those difficult situations as a project manager. I am very grateful for his guidance and wisdom during my time with the team.

I would also like to thank the Transportation Research Center for quickly moving this past spring to help me secure testing time at their facility to finish my thesis.

Dedication

This thesis is first dedicated to my parents and family. Without their guidance and support during my life, I would have never been able to reach my goals. They always taught me to never quit even when it gets hard and I am forever grateful to them.

This thesis is also dedicated to my wife Faith. Faith has taught me to appreciate all aspects of life and not just what you “have” to do to move forward. She has pushed me to be a better person and to listen to both myself and others for everything. If she had not uprooted her life and moved to West Virginia with me when I started at WVU I could have never had the mental strength to finish this research. I hope one day I can provide the same level of support for her.

Lastly, I would like to dedicate this thesis to my late grandfather. Grandpa overcame adversity in more ways than anyone could have ever imagined for a man who overcame polio at a young age. He would take what someone told him he couldn’t (can’t) do because of his disabilities and set out to do it. His attitude towards life, while quite brash at times, was to never let anyone tell you that you can’t and I hope I can have just a shred of that attitude as I move into life.

Table of Contents

Figures

Tables

List of Acronyms

ACC	Adaptive Cruise Control
ANL	Argonne National Laboratory
AVTC	North American Advanced Vehicle Technology
AWD	All-wheel drive
BLF	Binary logger file
BSFC	Brake-specific fuel consumption
CAN	Controller area network
CAV	Connected and automated vehicle
CD	Charge depletion
CSV	Comma-separated value
DBC	DataBase Container
DEI	Diversity equity and inclusion
DOE	U.S. Department of Energy
EBCM	Electronic brake control module
ECMS	Equivalent consumption minimization strategy
ECT1	EDU contribution test 1
ECT2	EDU contribution test 2
ECT3	EDU contribution test 3
EDU	Electric Drive Unit
EMC	EcoCar Mobility Challenge
EMF	Electromagnetic field
EPA	U.S. Environmental Protection Agency
ERAD	Electrified rear axle drive
ESS	Energy storage system
EV	Electric vehicle
EVC	EcoCAR Electric Vehicle Challenge
EVRE	EV with range extender
FDA	Functional Data Analysis
GM	General Motors
HEV	Hybrid Electric Vehicle
HIL	Hardware-in-loop
HS	High speed
HV	High voltage
ICE	Internal combustion engines
MIL	Model-in-loop
NDA	Nondisclosure agreement
PCM	Propulsion controls and modeling
PHEV	Plug-in hybrid electric vehicles
PM	Project management
PSI	Propulsion systems integration
SAE	Society of Automotive Engineers
SDI	System design and integration
SOC	State of charge

TCC	typical coastdown conditions/control
TRC	Transportation Research Center
V2X	Vehicle-to-everything
VIL	Vehicle-in-loop
WVU	West Virginia University

List of Symbols

Symbol	Description	Units
	English	
A	Frontal area	m^2
A	Roadload coefficient A	N
B	Roadload coefficient B	$\frac{N}{m/s}$
C	Roadload coefficient C	$\frac{N}{m^2/s^2}$
Cd	Coefficient of drag	-
F_{backEMFp}	Mback EMF force derived from battery power method	N
$F_{\mathrm{backEMFts}}$	Back EMF force derived from torque method	N
F_{Cd}	Force acting on a vehicle due to the air resistance	N
F_d	Force acting on a vehicle due to general disturbance	N
F_G	Force acting on a vehicle due to road grade	N
F_{rr}	Rolling resistance acting on a vehicle	N
F_t	Total force acting on the vehicle	N
F_{TR}	Total tractive force acting on the vehicle	N
$F_{windconst}$	Force acting on the vehicle due to a constant wind	N
g	Earth's gravity	m/s^2
m_v	Mass of the vehicle	kg
P_{batt}	Battery Power	W
t	Time	s
v	Vehicle velocity	m/s
$\dot{v}$	Vehicle acceleration	m/s^2
$V_{windconst}$	Constant wind velocity	m/s
	Greek	
α	Road grade angle	%
μ	Rolling resistance coefficient	-
ω_{motor}	Motor Speed	RPM
ρ	Air density	kg/m^3
τ_{motor}	Motor Wheel Torque	Nm

1. Introduction

The primary objective of the research is to compare the results of a set of experimental hybrid electric vehicle coastdown tests using previously unverified procedures. Knowledge of the actual vehicle coast-down results increases and establishes an understanding of the most accurate coast-down procedure for a hybrid and or electric vehicle. Having confidence in the vehicle's road load derived from a coastdown test increases vehicle model fidelity which leads to improved model-based engineering, vehicle plant model development, and vehicle controller development. Model-based engineering is the future of automotive engineering, and this research aims to take advantage of an available development hybrid electric vehicle to improve current and future vehicle models through an understanding of the best practice coastdown procedure for hybrid electric vehicles.

Vehicle manufacturers perform their own coastdowns, at their tracks, under their own conditions and specifications. Then they report their findings to the Environmental Protection Agency (EPA) for certification testing. Unfortunately for independent testers, this means lack of repeatability. In fact [1] found that the only way to corelate coastdown results was through the testing facility. For the case of independent testing, this means that results will almost never match manufacturer and EPA specified road load parameters. Therefore, it is needed to perform a new test at a new location to determine a vehicle's actual road load.

The motivation behind this work is driven by the West Virginia University (WVU) EcoCAR Team and its participation in the previous and current North American Advanced Vehicle Technology (AVTC) competitions the EcoCAR Mobility Challenge (EMC) and the EcoCAR Electric Vehicle Challenge (EVC). The EMC involved converting a 2019 Chevrolet Blazer into a hybrid electric vehicle (HEV) with a team-designed sensor suite with adaptive cruise control (ACC) [2]. The current AVTC, the EVC, involves the modification of a 2023 Cadillac LYRIQ with an emphasis on diversity equity, and inclusion as well as

connected and automated vehicle (CAV) algorithms [2]. This research will focus on the 2019 Chevrolet Blazer converted from a stock internal combustion to a hybridized powertrain for the EMC. This vehicle finished its life as a competition vehicle and now serves as a research and outreach tool for students. This research is also driven to benefit vehicle models and controller fidelity in the aforementioned EVC which utilizes a 2023 Cadillac LYRIQ as a competition vehicle. The statements earlier about the need to perform an independent test apply heavily to this team's success in the EcoCAR competitions. It is imperative that the team have knowledge of their specific donated vehicle's road load characteristics to properly simulate and model energy consumption and performance.

The history of HEVs, their different powertrain configurations, and torque split algorithms for parallel hybrid vehicles are discussed to provide a background to this research. The topic of hybrid vehicle modeling is discussed along with a brief development history. The history then leads to the general structure of the EcoCAR vehicle model of the 2019 Chevy Blazer as well as its torque split algorithm used for the EMC.

Coastdown testing is important to better understand a vehicle's kinetic characteristics during acceleration, deceleration, and constant speed events. A background in coast-down testing and hybrid and electric vehicle (EV) coast-down testing is explored along with the test procedure used for the current research. This paper presents results, conclusions, and general recommendations at the end.

1.1 Hybrid Electric Vehicles

HEVs are not a new concept with the first two documented concepts first shown in 1899 at the Paris Salon. The push for HEV research and development for the commercial market was spurred by Ford and GM with their sponsorship and participation in some of the first few AVTCs in the mid-90s [3]. The history of AVTCs will be discussed in a later section. The commercialization of the HEV is credited to Toyota Prius and Honda Insight and Civic vehicles in the late 90s and early 2000s [3]. Regardless of the

development and increase in manufacturing of HEVs, internal combustion engines (ICE) have been and still are the primary propulsion method for passenger vehicles in the United States. Approximately 90 percent of light-duty vehicle sales were ICE in 2021 [4]. The other 10 percent of sales in 2021 are comprised of HEVs and EVs with over 7.5 percent being HEVs (including plug-in hybrid electric vehicles (PHEV)). While this is certainly not a large percentage of consumer vehicles, it is a considerable increase in market percentage when compared to the 2.7 percent sold in 2020 [5]. The primary differences between HEV and ICE vehicles are the addition of a high voltage (HV) based propulsion system typically consisting of a battery pack and one or more electric motors that help move the vehicle in tandem with the engine. One of the largest reasons for the increase in HEV production and sales is the efficiency and environmental factors of hybrid and electric vehicles when compared to traditional ICE vehicles.

The tailpipe emissions of an HEV are typically lower than an ICE vehicle due to a torque split which optimizes the engine and electric components [6]. The well to wheels emissions of an HEV are also typically lower than an ICE vehicle due to the aid of the HV system which is isolated to the vehicle with no direct connection to the infrastructure [6]. The well to wheels emissions are important to mention as they represent a better portion of the lifecycle emissions. The efficiency of the typical optimal operating point of an ICE is roughly 30-40 percent whereas the efficiency of all the HV components of an EV or HEV can range from 65-95 percent [7][8] for the full system. HEV operation is focused on keeping the engine in the most optimal operation state at its lowest brake-specific fuel consumption (BSFC) points. To do this, the electric motor of the HEV is used to either provide more power to the system when needed, or it can opportunistically charge using regenerative braking to keep the engine at the most optimal point [9][10].

1.2 Hybrid Electric Vehicle Types and Architectures

There are three primary types (each can be broken down further if desired) of HEVs available to consumers today. HEV, PHEV, and EV with range extender (EVRE) are the three types. The HEV is a typical hybrid vehicle with a smaller energy storage system (ESS) than a PHEV or a full EV which uses its engine and an electric motor in tandem to deliver on a driver's torque request. Typically, the torque is split fairly equally between the two systems for an HEV with modifications at lower or higher vehicle speeds dependent on the torque request. The second most common type of hybrid is the PHEV. A PHEV's ESS can be charged at night to improve this vehicle's range during normal operation. A PHEV has two modes, a charge depletion (CD) EV-only mode until a certain ESS state of charge (SOC) then an operating mode that mimics that of a standard HEV. The final primary type of hybrid vehicle is an EVRE. An EVRE is charged similarly to the PHEV but uses a little bigger ESS and motor than a typical HEV and PHEV and a smaller engine to help supplement the HV system when needed. The EVRE has gained popularity more recently with many consumers suffering from range anxiety from a typical EV [11]. The 2019 Chevrolet Blazer used for this research is a standard HEV and its architecture will be discussed later.

If you were asked to design a "standard" HEV and provided no more information by a client, there are many different methods to accomplish this task. The two primary architectures for HEVs are series and parallel architectures. A series architecture utilizes a mechanical connection between the engine and the HV system. The engine is used to turn the generator which charges the ESS which powers the motor which is the primary propulsion method similar to an EV [12]. A parallel hybrid does not use a mechanical connection between the engine and the electrical components, only controllers or a "through-the-road" connection [13]. The primary goal with the two propulsion systems in a parallel HEV architecture is for both to operate in their most optimum region of the engine map at all times if possible [12]. The vehicle used in this research is a style of a parallel hybrid vehicle. In total, there are six

different motor location designations of hybrid vehicle architectures shown in Table 1. It is important to note that combinations of the locations can occur.

Table 1: Hybrid vehicle architecture motor location designations derived from Santis et al.[14]

Location	Location
P0 – Belt-driven motor/generator	In parallel with the engine serpentine belt on the accessory side of the engine, can be connected with a belt or chain
P1 – Motor replaces the engine flywheel	Upstream of clutch on the engine side and coupled to the same axle as the engine
P2 – Motor downstream of clutch	Downstream of the clutch but before the transmission and coupled to the same axle of the engine
P3 – Motor downstream of the transmission	Downstream of the transmission but is coupled to the same axle as the engine
P4 – Motor independently on the rear axle	Rear axle (not mechanically coupled)
P5 – In-wheel motors	Wheel (hub) motors not coupled to an engine or transmission

Out of the 6 different architectures, only the P4 and P5 architectures do not have a mechanical connection to the ICE on the other axle. The other 4 involve some form of mechanical connection between the EM and the engine. The vehicle used in this research is a P4 architecture. Hub motors can be used as a P3 architecture based on its definition even though Table 1 only highlights one of their uses.

1.3 Advanced Vehicle Technology Competitions

In the late 1980s, The U.S. Department of Energy (DOE) requested ideas and concepts to increase competitiveness and trade. The most successful idea of the idea workshop resulted in funding for a university competition sponsored by the Society of Automotive Engineers (SAE), Argonne National Laboratory (ANL), and the DOE to develop an energy-efficient vehicle using alternative fuel. The Methanol Marathon was officially the first Advanced Vehicle Technology Competition (AVTC) in 1988. Over the course of the next 35+ years, there have been 13 different AVTCs [2]. The two most recent AVTCs are discussed below.

1.3.1 EcoCAR Mobility Challenge

The EcoCAR Mobility Challenge (EMC) spanned 2018 to the spring of 2022 with 11 participating universities. The overall goal of the EMC was to hybridize a stock 2019 Chevrolet Blazer donated by General Motors (GM) to increase the efficiency of the vehicle while also maintaining the stock performance. A secondary goal of the EMC was to design an Adaptive Cruise Control (ACC) algorithm which interfaced with the environment using a sensor fusion algorithm and vehicle-to-everything (V2X) capability with a goal of SAE Level 2 automation [15]. At the end of each year, teams competed with their vehicles and presented their engineering design process.

Each university team had 5 different swimlanes to design, build, and test their Chevrolet Blazer over the EMC. The project management (PM) swimlane consisted of a graduate student leader and a small team dedicated to planning and tracking the overall project transcending semesters and project years. The PM reported to the faculty advisors and GM mentor and then interfaced with each of the 3 other technical swimlane leaders and their respective teams. The other non-technical swimlane was the communications swimlane which focused on outreach events and general project promotion through

social media. The technical swimlanes are the propulsion systems integration (PSI) team, the propulsion controls and modeling (PCM) team, and the connected and automated vehicle (CAV) team.

The PSI swimlane's primary role is the integration process of the vehicle. This involved a drivetrain swap between the stock ICE/transmission and smaller donated ICE/transmission, HV system integration (HV ESS, inverter, and motor), and all wiring of the vehicle in the initial years of the competition. In the later years of the competition, the PSI swimlane handled the final vehicle calibration (in parallel with the PCM swimlane) and final mechanical refinement as needed. The PCM swimlane handled vehicle modeling, the controller development (including an energy management strategy), and helped determine a proposed architecture in the first year of the competition based on their simulation results. The PCM team also performed extensive model-in-loop (MIL) and hardware-in-loop (HIL) testing to develop a robust limit and fault analysis system to protect the team's integrated components during vehicle-in-loop (VIL) testing. This ensured a productive use of the competition vehicle and track time when finalizing the overall system. The CAV swimlane's primary focus during the EMC was to develop a sensor fusion algorithm that interpreted camera and radar data to then provide accurate information to the ACC algorithm regarding a lead vehicle's distance and speed from the ego vehicle. The CAV team also worked with Cohda radios to communicate with stop lights and stop signs to inform the ACC algorithm when, how much, and if to slow the vehicle when it approaches an intersection.

1.3.2 EcoCAR EV Challenge

The EcoCAR EV Challenge (EVC) began in the Fall of 2022 and is currently proposed to take 4 years with a competition at the end of each year. The overall goal of the EVC is to engineer a next-generation battery electric vehicle with a focus on improving the automation and V2X concepts explored during the EMC. Each team will be provided a 2023 RWD Cadillac LYRIQ to modify with advanced propulsion strategies

and energy management methodology in parallel with connected and automated vehicle (CAV) technologies [16].

The EVC started with a similar team structure as the EMC. The three differences are the naming convention of the PSI team to the system design and integration (SDI) team, the addition of a diversity equity and inclusion (DEI) team and graduate student leader, and the fact the competition organizers chose to change the naming convention from swimlane to subteam. Otherwise, the general team structure and responsibilities remain the same as the previous competition. As this research is focused on a continuation of the EMC as the EVC is only just finishing its first year, there is not much fully defined for the later years except for guaranteed year-end competitions and presentations.

It is important to mention the EVC as it is one of the motivations behind the current research. Upon receiving the donated Cadillac LYRIQ, the team will have also received GM's stated road load for the vehicle. This topic will be explored shortly, however, it is important to mention that the team will need to benchmark their donated vehicle to determine the actual road load at the localized testing locations available. This is important to effectively generate a more accurate vehicle model for vehicle performance predictions including energy consumption and acceleration metrics.

1.4 WVU Chevrolet Blazer Vehicle Architecture

As mentioned previously, the 2019 Chevrolet Blazer was converted from a stock vehicle to a hybridized Chevrolet Blazer. The team architecture discussed in detail is pictured in Figure 1. Powering the front axle is a GM 2.5L LCV engine which replaced the stock 3.6L engine. The maximum torque of the 2.5L engine is 255 Nm and it has a maximum power output of 148 kW. This engine is mated with the GM 9-speed M3D 9T50 transmission. WVU chose this power cube for the front axle as it is a stock configuration in a lower-trim 2019 Chevrolet Blazer leading to improved mounting capability due to available stock GM mounts and accessories. While other university teams opted for the addition of a

turbocharger, WVU found that the chosen power cube was the lowest risk. To hybridize the donated Blazer, the rear axle was fitted with a MAGNA electrified rear axle drive (ERAD) system supplied by the GM HEV4 battery pack ESS. The HEV4 battery pack is a 1.5 kWh ESS with a pack voltage of 300 V and a maximum power output of 50 kW. The supplied P4 drive unit has a peak power output of 60 kW and a continuous power output of 20 kW which ensured the team would not need to worry about power limits between the ESS and the motor. The MAGNA ERAD's maximum torque is 200 Nm with a maximum continuous torque value of 90 Nm and a final drive ratio of 9.17:1 [9], [10].

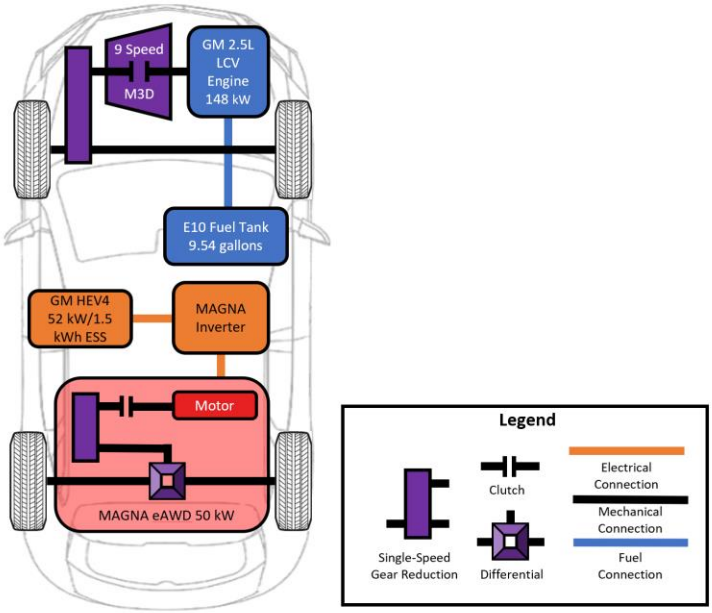

Figure 1: WVU Hybridized Chevrolet Blazer Architecture

At the end of the EMC, the WVU Blazer had multiple modes of operation. The first mode of operation was an ICE-only FWD mode of operation where the rear axle of the vehicle was completely disconnected using an integrated clutch. The disconnected rear-axle FWD motoring mode is not the common operating mode for the vehicle. This mode was utilized as a backup mode to the standard AWD hybrid operating mode. The standard AWD mode contained two sub-modes. In a standard motoring situation, propulsive torque is commanded to both the front and rear axle through the team-added controller.

That torque split was arbitrated and determined by a team-implemented equivalent consumption minimization strategy (ECMS) to determine the most optimal split of commanded torque. Based on the ESS SOC and torque command, the ECMS algorithm would determine when opportunity charging AWD operation was needed. Opportunity charging primarily occurs when the SOC is below the ECMS target SOC. In this mode of operation, positive torque is commanded to the front axle and negative torque to the rear causing the motor to effectively drag and charge the ESS. The last primary method of operation is a one-pedal-like driving feature the team chose to implement as a consumer appeal feature during the final year of the EMC. When the driver is approaching an intersection or a stop, they can release the accelerator pedal and the pedal map commands a "large" negative torque to the rear axle which slows the vehicle at a rate similar to a soft braking event.

A pedal map is a matrix of torque commands based on vehicle speed and accelerator pedal position. In the scenario of normal operation, a positive torque command is the primary output of this matrix. During a coasting event, when the accelerator pedal position is zero, the WVU team calibrated this specific row of the pedal map to output a negative torque to the vehicle. This calibration was based on a combination of driver comfort and maximum energy recapture. The ECMS algorithm then switches states to transfer the total negative torque command to the rear axle.

1.4.1 Equivalent Consumption Minimization Strategy

The ECMS algorithm has a rich history in the HEV controls space as well as at WVU [10], [17]. ECMS was originally introduced in 1999 as an instantaneous minimization problem based on energy flow through the system. One of the primary assumptions of ECMS is that the HV system acts as an aid to the IC engine and can be treated as an "extra" fuel tank in the overall system. With this assumption in mind, ECMS algorithms equate stored battery energy to fuel energy and then compare this fuel energy to the actual fuel energy present in the fuel tank. The optimal torque split of a parallel HEV is determined by

the smallest equivalent fuel consumption at that instant in time [18]. It is important to note that the most optimal split at each instance in time may not be attainable due to the large error from the previous torque value of the component. The most important aspect of ECMS is how it compares actual fuel consumed to an equivalent fuel consumed by the vehicle's electrical components.

As the WVU EcoCAR team implemented this torque split strategy as part of its controller, it is important to mention the background of the ECMS algorithm. However, this research does not modify or adapt the torque split strategy of the Blazer. Further reading about the ECMS algorithm and other torque split algorithms is found in [9], [10], [17]–[20].

1.5 Hybrid Vehicle Modeling

Vehicle modeling is not new to the vehicle design and engineering community yet more companies are focusing on improving their modeling resources to improve workflow and time saved. It is a means to collect data and make engineering judgments that would otherwise use unnecessary time and resources. A prototype vehicle can cost over 200,000 USD. With this cost simply associated with the build itself, vehicle modeling can save valuable money, time, and effort from engineers [21]. The world of hybrid electric vehicle modeling expanded greatly in the 1990s with MATLAB and Simulink models of series HEVs yielding results within 10% of experimental data [22]. During the late 90s, various researchers, and AVTC competition teams developed the fundamental Simulink block sets and vehicle modeling methodologies which are still in use today. As other technologies in the automotive industry advanced, so did vehicle modeling techniques. Moving into the modern era, in 2022 MathWorks released their Virtual Vehicle Composer which generates a basic vehicle model for the user automatically with knowledge of some basic vehicle parameters [23]. This enables the quick creation of a vehicle model for a rapid development environment. There are advantages and disadvantages to this rapid model development. One advantage is quick "back-of-the-hand" calculations for future vehicles a

company might want to develop are now expedited in a more useful setting with analytical drive cycle results. A disadvantage is an inherent trust an engineer could develop towards the model where they treat auto-generated subsystems as “black boxes” and assume the results must be right because Simulink can not possibly be wrong. This lack of understanding of the source code and how the model truly determines the vehicle response could lead to careless mistakes in the near future.

1.6 Coastdown Testing and Road Load Measurement

Coastdown testing is an integral part of any vehicle development process. This testing supplies an engineer with crucial knowledge of a vehicle’s overall rolling losses. These rolling losses are used in a variety of applications. One such application is vehicle modeling in the software environment. Another application of the rolling losses is vehicle dynamometer calibration. In 1976 an SAE task force was compiled, and they developed the standard practice J1263 which became the original source material for road testing to determine a vehicle’s road load and then translate those results into vehicle dynamometer testing. Understanding and reducing the road load of a vehicle is extremely important for the efficiency and longevity of any size vehicle [24]. The coastdown test at a high level is taking the intended test vehicle to 75 mph and placing the gear selection in neutral to coast the vehicle with no additional drivetrain losses from the transmission until the vehicle speed is less than 5 mph. During this stint, vehicle speed and distance over time are recorded for further evaluation [25]. The idea of Coastdown testing is derived from Newton’s second law of motion which at a high level explains a coasting vehicle’s motion in a straight line. The force acting upon a vehicle is proportional to the mass of the vehicle and the rate at which the vehicle is decelerating. Therefore, the overall forces acting on a vehicle during a coastdown test are proportional to the mass multiplied by the time rate of change of the velocity of the vehicle. Before a coastdown test can even begin, there are strict requirements regarding vehicle occupants, vehicle conditions, environmental conditions, and instrumentation resolution.

To understand why a coastdown test is the most effective method to accurately comprehend the overall forces it is important to visit the free-body diagram of a vehicle as it is moving in a direction as shown in Figure 2. The resulting analysis of the free-body diagram is a direct application of Newton's second law. The vehicle pictured is a representation of the EcoCAR 3 AVTC which focused on converting a 2014 Chevrolet Camaro into an HEV [26].

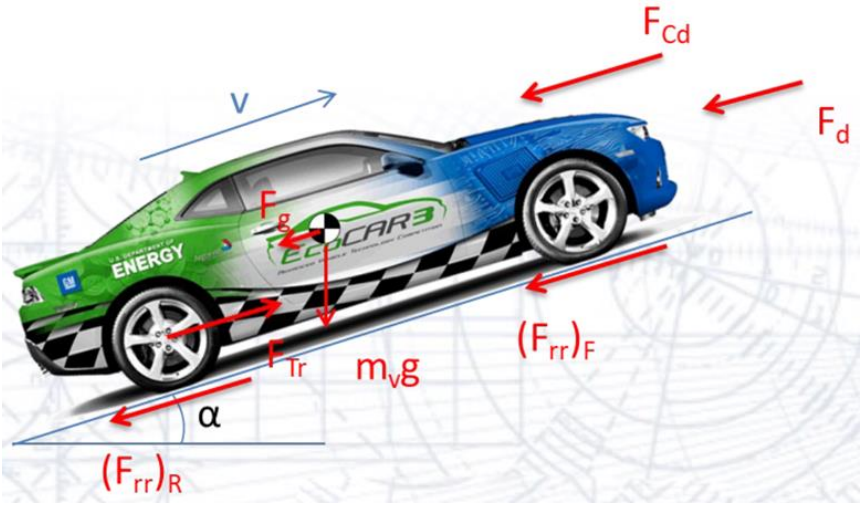

Figure 2: Free-body-diagram of a 1-dimensional representation of a vehicle [27].

Application of Newton's second law in the direction of the vehicle's travel yields Equation (1) below:

$$F_t = m_v \dot{v} \tag{1}$$

Where F_t represents the total force acting on the vehicle at any given time *t.* The mass of the vehicle m_v is then multiplied by the vehicle's acceleration $\dot{v}$. The total force acting on the vehicle can be further broken down into its components. Equation (2) shown below documents the various components of the total force.

$$F_t = F_{Tr} + F_{rr} + F_{Cd} + F_G + F_d \tag{2}$$

Where F_{Tr} represents the tractive force propelling the vehicle in the positive x direction. During a coastdown event, the tractive force is roughly zero and the total force acting on the vehicle is equal to the force due to the rolling resistance F_{rr}, the force due to the air resistance F_{Cd}, the force due to road grade F_G, and the force due to general disturbance F_d. The general disturbance forces are reflected through the back EMF forces discussed later but will be removed from this equation for now. Expanding the force terms yields Equation (3) below.

$$F_t = \mu m_v g + \frac{1}{2} C_d \rho A v^2 + m_v g sin(\alpha) \quad (3)$$

The force due to rolling resistance is comprised of the rolling resistance coefficient μ and the weight of the vehicle mg. The force due to the air resistance is defined by the drag equation [28] where C_d is the drag coefficient, ρ in the density of air at the testing temperature and pressure, A is the frontal area of the vehicle which is typically a factor of 0.8 multiplied by the rectangular base and height as viewed from in front of the vehicle [29], and V is the velocity. The final term in the total force is the force due to the road grade which is represented by the weight of the vehicle corrected for the angle of the road α. For optimal coastdown testing, the road grade is neglected due to a straight flat test track.

Terms defined in Equation 3 can then be back calculated from a vehicle's road load versus velocity curves to be imported into a Simulink vehicle model to better represent a specific vehicle in a modeling environment. The most versatile part of this activity is the user does not even need to truly know the parameters in Equation 3. If one derives a second-order polynomial curve fit of the force versus velocity curve of a coastdown, the three terms can be imported into the Simulink block "Vehicle Body Total Road Load" as shown in Figure 3.

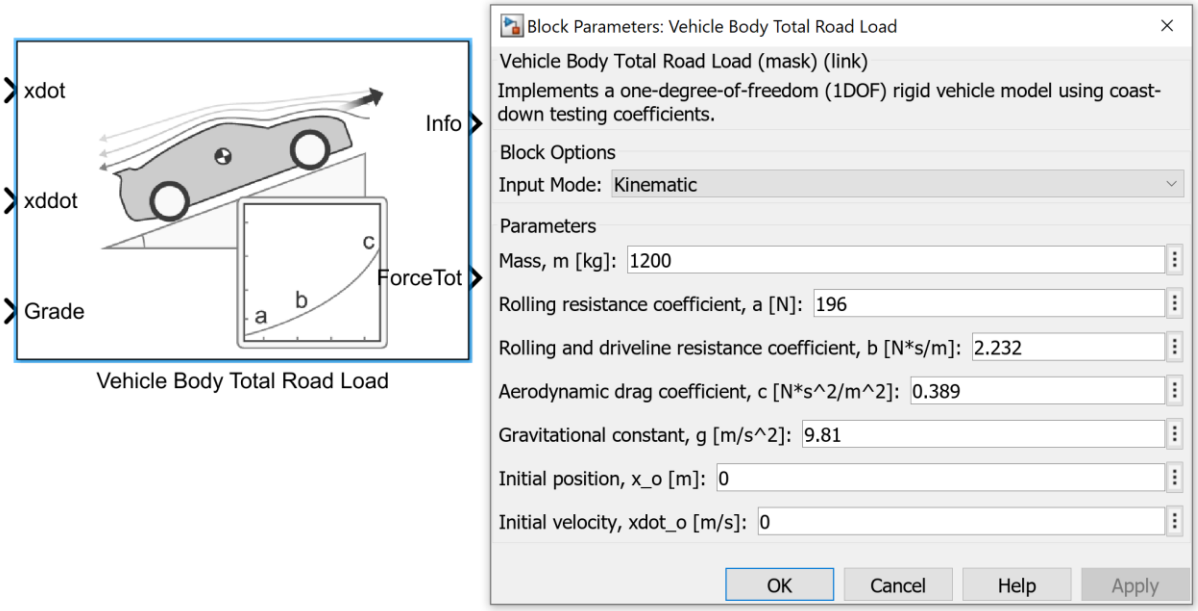

Figure 3: Simulink Vehicle Body Total Road Load

All three terms in the second order polynomial fit are represented here by “a”, “b”, and “c”. Where “a” is the 0^{th} order term, “b” is the 1^{st} order term, and “c” is the 2^{nd} order term of the fit. These three terms are used in common practice amongst certification testers and vehicle developers for dynamometer testing as the loading parameters for drive cycle testing of a vehicle. Knowing the correct road load of a vehicle ensures improved accuracy for energy consumption results and truthful emissions results for the case of hybrid vehicles.

2. Literature Review of Coastdown and Road Load Experiments

The sections in this literature review provide an overview of previous work in road load determination through coast-down testing and its application. More specifically it focuses in on the previous works in the hybrid vehicle environment when applicable. While there are notable works prior to the 1970s, it was determined that a high-level analysis of notable works over the past 50 years is sufficient for this research and only one work from the 1960s is notable.

2.1 1960s

The University of Washington, in 1964, set out to determine the road load of large trucks in an effort to understand the actual forces acting on vehicles for fuel economy reasons [30]. This study determined that the best method for determining the load was a coastdown test from 60 mph to 30 mph using a data splicing method as the available section of the highway was not long enough for a longer run. The study used 5 Class 8 trucks and 1 passenger car for their experiments. Due to the year and the technology available, the authors did note a few shortcomings with their obtained results. The first shortcoming they mentioned was potential accuracy issues with acceleration derived from the vehicle's speedometer. Another shortcoming they attempted to address and mentioned should be standard practice in later years was to ensure all rotating components are "warmed up" before testing to prevent damping changes due to temperature variation.

2.2 1970s

In 1972, the University of Illinois set out to determine the coefficient of drag and rolling resistance for a variety of vehicles by isolating the parameters mathematically from the vehicles' coastdown results [31]. The study examined 7 different vehicles and chose to derive the coefficient of drag and rolling resistance without differentiating the velocity profile of the vehicle. The coastdown tests were from approximately

75 mph to 20 mph. The final results showed a good closeness of the calculated coefficient of drag to previously posted values for the same vehicles and the researchers concluded that the mathematical model used to calculate the coefficient of drag and rolling resistance is acceptable.

In 1977, the EPA conducted a series of coastdown tests as one of the first large tests to determine vehicle road load. The primary goal of this study was to efficiently predict the road load of various light-duty trucks to aid in predicting dynamometer load settings for future emissions testing [32]. The study used 15 different trucks and vans testing at the Transportation Research Center (TRC) with varying loads in each truck equating to 50 coastdown tests on the TRC's oval track. The study analyzed the correlation between vehicle mass, vehicle inertia, and frontal area versus vehicle road load. The study concluded that it is more beneficial to predict vehicle road load using the frontal area over the vehicle's mass [32].

In 1978, GM conducted a series of experiments to help determine the theoretical basis to successful coastdown testing as well as the approach that should be taken. One of the key takeaways from this testing was the effects of wind speed on correlation coefficient determination. GM determined that light wind is acceptable for coastdown testing, but high winds, especially crosswinds, are detrimental to results determination. One such finding was that it is not acceptable to determine rolling resistance in high wind scenarios [33]. The study by GM is a good baseline approach to understanding how wind and ambient temperature conditions could impact coastdown testing.

GM conducted another road load study in 1978 which focused on the effects that road surface has on the coefficient of rolling resistance [34]. Using a roller system, they analyzed two vastly different surfaces and multiple tire constructions to confirm that rolling resistance is much higher on a material that mimicked 80-grit sandpaper versus smooth steel. The rolling resistance tests were conducted at a constant speed to isolate the losses and compare the surfaces at one speed. On the outdoor tests, with

a single tire mounted onto a moving vehicle, they found that as road surfaces increased in roughness, the rolling resistance could increase by over 30%.

2.3 1980s

In 1981, GM performed a study that analyzed the SAE standard J1263 (new in the late 1970s) and sought to replicate the methodology proposed and suggest improvements for future testing [24]. The study discussed the implementation of the two-part method outlined in J1263 where a combination of road and dynamometer tests are used to properly set the force on a dynamometer. This study suggested improvements to the method outlined in J1263 by performing the dynamometer tests over a range of speeds instead of the suggested window of 88 – 72 kph. The study also suggested that 100 - 30 kph is a sufficient vehicle speed range for coastdown testing based on the suggestions of all contributing parties to SAE J1263. The author also provided advantages and disadvantages for 6 different road load determination testing methods split between steady-state testing and free deceleration testing. At the end of the comparison, they still suggest the speed versus time standard coastdown proposed in SAE J1263 as the best method for obtaining the vehicle road load.

Northrop and the U.S. EPA conducted a series of coastdown tests in 1983 with Class 6 delivery vehicles with the goal of creating analytical models with varied complexity [1]. The study assumed zero grade with all coastdown tests and focused instead on other parameters. The study aimed to focus on and isolate the frictional forces of the test trucks. To account for mechanical and electrical noise in the final coastdown curve, the group smoothed the raw data with a quadratic fit and then differentiated every 2 seconds to obtain the deceleration over time curve. They also noted that the smoothing had negligible effects on the results. This study analyzed 4 different models all with varying complexity and determined that the 3 term model used by the EPA was the most appropriate for road load determination.

In 1989 a group from the University of Saskatchewan conducted over 100 coastdown tests in windy conditions and varying grades with the goal to develop test methodology for atypical testing conditions for future coastdown tests [35]. The group used a vehicle that was deemed the worst-case scenario for determining vehicle rolling resistance, the Nexus three-wheeled prototype which was created to improve efficiency and safety for single-person travel. The study explicitly selected a test track with varied grades of over 5 meters and performed testing in windy and non-windy conditions to mimic the worst-case scenario road load determination testing. The group based their coastdown procedure rules on SAE J1263 to ensure repeatability and consistent test procedure across all coastdown runs. Like other coastdown tests, the relative airspeed of the vehicle was monitored along with other typical parameters during each run. A total of 80 tests were performed in windy conditions and another 68 in calm conditions. For the calm condition testing, the yaw angle on the vehicle was assumed to be zero. The study found that a method for testing in windy and high-grade conditions is viable. However, the study did conclude that the high wind conditions led to a higher standard deviation in results.

2.4 1990s

In 1990, the University of Illinois conducted an analysis and comparison between the two-term approximation of the road load as proposed by J1263 and a three-term approximation [36]. The three-term approximation is derived from the Davis equation and was used in other studies involving the coastdowns of locomotives. The authors' desire to improve the approximation of the aerodynamic drag terms of the road load equation led them to use the three-term approach in a comparative analysis against the two-term approach in two different computer programs. The first program they used was a generating program that created arbitrary coastdown results based on known vehicle parameters. The other type of program used was an evaluation program which accepts coastdown results and performs the required post-processing. The authors found that the two-term approximation established in previous tests is sufficient unless you desire delineation of the drag coefficients.

The University of Maryland, in 1995, studied potential improvements to the standard coastdown procedure by including an onboard anemometer to increase the precision of the force due to drag term in the road load equation [37]. The group developed a new algorithm for coastdown testing and analysis they called the "ABCD" method or the Anemometer Based Coast or Drive method. The group developed 8 different assumptions for the ABCD method which surround neglecting potential micro changes due to winds or tire slippage in their results. For testing, the anemometer was placed on a boom mounted to the front bumper. The boom was approximately 2 meters in front of the vehicle and the anemometer was approximately the same height as the crown of the vehicle's hood. The study used 8 different aerodynamic configurations, 3 different mechanical configurations, and 3 different vehicles to conclude that their procedure was repeatable and provided good results.

In 1996, the SAE developed the newest standard testing procedure for coastdown testing, J2263. The primary goal of SAE J2263 was to supplement SAE J1263 and improve its procedure for higher wind conditions [38]. Through multiple different studies, including some referenced in this work, the group determined that a new supplementary standard was needed. The notable addition to this standard is the request for vehicle-mounted wind speed and ambient temperature sensors. While there are no results for this work, it is important to mention as almost all modern coastdown work follows the procedure outlined in J2263. On that note, modern coastdowns still follow the original procedure from J1263 but with the modifications in J2263.

A coastdown test was performed on a Formula 1 car in 1996 via a joint effort from Loughborough University and the Benetton Formula 1 team [39]. The goal of this study was to conduct a coastdown test on Benetton's Formula 1 car using the methods developed at Loughborough University to develop an accurate mathematical model of this specific car's road load. The group conducted 4 coastdown tests at a Grand Prix track at different wind speeds and then compared those results to wind tunnel and tire rig results. One significant difference between the tire rig testing and the track testing is that at the

track, they could not put the car into neutral and had to instead just press in the clutch. The final results showed promise with the higher order terms but the 0^{th} order term of the three-term road load equation yielded a 30% difference between lab and track results. However, the group determined that the results were sufficient to develop the mathematical model.

In 1997, the Central Scientific Research Automobile and Automotive Engines Institute in Russia proposed and tested a modification to the measurement method of the standard coastdown test by measuring distance versus time instead of velocity versus time [40]. Through the integration of the road load equation presented in previous works discussed, this study determined an equation that related the three terms (dubbed a, b, and c) in the three-term road load equation to the distance the test vehicle traveled over time. The group established 4 known points on the track and measured the time at each point to determine the distance versus time vector needed for the analysis. After testing over 23 different vehicles, the authors concluded that the method of measuring the time between known distances is an adequate method of determining vehicle road load.

2.5 2000s

A study in 2001, by Sverdrup Technology and DaimlerChrysler (now Stellantis), sought to determine an accurate correlation between wind tunnel results and coastdown test results to aid in future vehicle road load approximation [41]. The group was driven by DaimlerChrysler requirements on the uncertainty range of the CdA values of their vehicles. The study used 3 different Dodge vehicles and drag plates for a total of 9 different vehicle configurations. For their coastdown testing, the group used the "ABCD" method described in [37] for their procedure. To add randomness, the group alternated vehicles and drag plates at different times during the day to capture a variety of ambient conditions. This same procedure paired with their previous experience was produced for the wind tunnel testing. The group found that they were able to predict CdA values within 4% which met their requirements.

Another coastdown to wind tunnel comparison was performed the following year in 2002 by Land Rover and Loughborough University using the same prototype Land Rover vehicle in 5 different configurations [42]. One thing to note is that while the procedure was similar to [41], the group notes some uncertainties may be present due to the coastdown data collection occurring over the course of a year and not at the same time. This added considerable uncertainty to their CdA values obtained from their coastdown testing.

In 2003, researchers at the University of Stuttgart introduced a driving-torque method measurement methodology to measure individual road loads [43]. The group chose to highly instrument the vehicle and add a streamlined trailer for a robust measurement suite to isolate each component of the road load equation. In order to isolate certain aspects of the road load, the team chose to perform tests at a steady state between 110 and 150 kph dependent on the speed of traffic on the Autobahn. The team found a 1% variation in their coefficient of drag term which is an example of why the group chose to test at a steady state. Due to the custom-tailored trailer and the test measurement method, the authors do make a note that this method is difficult to achieve for a fleet of vehicles needing testing.

This next study by Warn Industries in 2005 is not necessarily geared toward coastdown testing but is vital to understanding potential energy loss differences between a similar system using a disconnect method to switch between 2wd and 4wd [44]. The study focused on providing the background reasoning for their exploration and justifying their work based on the understanding that if an axle is completely disconnected from the wheels, the drivetrain is not spinning equating to minimal to no losses at that moment. The group then derived a series of energy equations that could be used in future studies. While this study did not have tangible laboratory work to back their research, they did lay the groundwork for future studies on the effects a disconnect clutch might have on a 4wd or AWD vehicle.

2.6 2010s

In 2011, a group from Ford Motor Company developed a testing framework for correlating in-vehicle test results to a Simulink-based vehicle model of HEVs [45]. While this work does not explicitly state a defined procedure for coastdown testing of HEVs, they do outline vehicle testing best practices for HEVs at Ford and make those suggestions to others. The study tells the reader that (intuitively) for noise reduction in the statistical analysis of the data, consistent testing following their outlined suggestions must be followed. In order to accomplish a valid correlation, the study suggests 26 parameters to monitor during vehicle testing.

The Netherlands Organization for Applied Scientific Research (TNO) in 2012 published a comprehensive work that aimed to compare the European Type Approval testing for vehicle fuel consumption and real-world results [46]. The study evaluated 6 Euro-5/6 vehicles and 2 Euro-4 vehicles which were the same model as the newer Euro-5/6 vehicles. For all coastdown testing, the group ensured to run in opposite directions to negate wind effects. Unlike other tests, the research followed the procedure outlined in UNECE R83 which is the European Union's standards for type approval and road load determination. One example if the differences is that UNECE R83 uses time instead of force for the initial data and then later converts it to a force measurement. In the end, they still determine the three-term road load equation as seen in many studies. After running emissions testing with the group's tested road load coefficients, they found an average 24% increase in emissions over the manufacturer's stated emissions. This is however pre-emissions scandal that occurred in 2015 and there is no statement in this report of the model of the vehicles used for testing. The group does disclose that a few of their tested vehicles are diesel. While this work does not regard a variable vehicle mass, it is still imperative to understand its effects on road load coefficients. The group reported a significant increase in the road load coefficients as mass increased at lower vehicle speeds. Their findings suggest that mass reduction is imperative to reducing vehicle road load.

A 2013 study funded by the U.S. Department of Energy and led by Carlson from Idaho National Laboratory studied the effects of vehicle mass on three different vehicle architectures: ICE, HEV, and BEV vehicles [47]. The group tested three vehicles. Two of the three vehicles were the same make and model except for one was an ICE and one was an HEV trim package, and the final vehicle was a smaller BEV. With each of the three vehicles, the group performed 14 coastdowns at each of the 5 different weight points on a two-mile straightaway in Arizona. After performing the coastdowns, the determined road loads were used on a chassis dynamometer for energy consumption testing. The study deduced that there is a non-linear decreasing trend in the road load coefficients when mass was decreased linearly. The group also determined that this trend was consistent for all three test vehicles. One interesting aspect of this study is the uncertainty present with the coastdown results of the HEV and the BEV. For each vehicle tested, there was no true mechanical neutral. This study was not focused on these effects and one of the primary goals of the research presented in this paper is to fill this gap.

In 2015, the basis behind this research was developed by Intertek in partnership with Center for Evaluation of Clean Energy Technology (CECET) through a test specification to determine the road load through coastdown testing [25]. The group developed their test procedure in accordance with SAE J1263 and J1711 to specifically support advanced vehicle testing and development road load determination. Most of the proposed coastdown procedure is standard compared to other research in this literature review. Where this work differs from the others is their recommendations for performing coastdown testing with electrified axles. More specifically BEV and HEV contain an electrified axle that does not have a mechanical neutral and/or the vehicle does not have a zero torque state for the axle. The group's suggestion for vehicles that met this criterion is to calculate the counter-electromotive force (as defined by the author, more commonly known as the back electromagnetic field (EMF) force) of the motor(s) with respect to the vehicle's velocity and subtract that force from the total road load. Equations (4) and (5) below document the two methods of calculating the back EMF force during the data reduction of

coastdown testing. These two equations will be pivotal in this research's data reduction and road load determination process.

$$F_{backEMFts} = \frac{\tau_{motor}\omega_{motor}}{V} \quad (4)$$

$$F_{backEMFp} = \frac{P_{batt}}{V} \quad (5)$$

The first method of calculating the back EMF force uses the torque at the motor at the wheels multiplied by the motor speed and then divide by the vehicle speed. The second suggested method is to take the voltage and current values to calculate the power output by the battery and divide it by the vehicle speed. Either method can be used dependent on the signals measured during testing. For the WVU Blazer, all signals specified in Equations (4) and (5) are monitored on the team's added CAN bus. Other than the modifications for EVs and HEVs, this study has little to no differences from other coastdown standards in terms of procedure and data analysis.

A study in 2015 by Roskilde University Center in Denmark explored how road surface characteristics influenced road load while also using a new Functional Data Analysis (FDA) methodology for data reduction [48]. The group's data was derived through a previous study but contained 28 different strips of the road using the same vehicle, a Volvo 940. On each road strip the group averaged 15 runs and used reflective strips at known distances to capture the vehicle's velocity. Through the study's development of different models, they found that for most cases, each model was only viable for each specific strip of road. This prompted a suggestion of future work to improve their modeling process as their force due to rolling resistance was inconsistent within their modeling.

The Korea Automobile Testing & Research Institute and Korea University in 2016 performed a study with the goal of determining the key factors that affect the road load determination from coastdown testing

to better understand the manufacturer's claimed road load coefficients [49]. The key factors focused on why a third-party testing agency might obtain different road load coefficients than what a vehicle manufacturer tells the government. For this study's coastdown testing, they used a split run approach with one test vehicle loosely following SAE J2263. To simulate the testing being performed by a third party, the group would switch test drivers and test sites during experimentation in order to see what effect that might have on the results. From their statistical analysis, the group determined that one of the only statistically relevant factors when comparing manufacturer-obtained road load coefficients and third-party-obtained road load coefficients is the test site where the coastdown is performed.

In 2017, The EPA and NVFEL performed a road load study aimed at exploring the differences between obtaining a vehicle's road load coefficients through coastdown testing versus through a steady-state method [50] similar to [43]. Their study was specifically aimed at adapting the traditional coastdown test to be more inclusive of HEV and EV vehicles that may not have a true mechanical neutral often needed for coastdown testing. Using a GM Volt EV, the group performed coastdown testing and steady-state speed testing at the same test facility. They measured parameters using the vehicle's CAN as well as other methods (current clamps, voltage taps) and performed a comparison before analyzing the collected data. The comparison did conclude that the CAN bus monitoring is a reliable method of collecting data for these tests. The group then repeated the coastdown and steady-state testing on a chassis dynamometer. After performing their data analysis, the group concluded that steady-state speed testing is a valid method for determining the road load on vehicles that do not have a true neutral.

A later study in 2014 by Kidambi et al. dynamically varied the road load based on a variable vehicle mass. Essentially their algorithm can be used to change the reported road load to modify suspension or transmission shift maps while the vehicle is in motion.

Vehicle mass through the reduction of the road load coefficients also has a direct positive impact on energy consumption and the projected range of electric vehicles as found by Joost in 2012. While this particular paper will not focus on the impact of mass on the road load coefficients, it is still imperative to understand the impact a variable mass may have. The mass will need to be constant through all coast-down testing to prevent unnecessary data variability.

2.7 2020s

In 2020, Moskalik through the EPA performed an experiment in benchmarking various vehicle transmissions, including using a coastdown test [51]. The findings were later used for correlation purposes to accurately predict the contribution of neutral losses in various transmissions for on-the-market vehicles. The experiment used 5 different transmissions found on typical vehicles on the road today. To isolate variability and focus on the transmission itself all data was collected in a small engine test cell using a dynamometer and commanding the engine to different speeds to simulate a coastdown. One thing to note from their testing was that two more modern transmissions with active controls and shifting characteristics did not have the same second-order behavior as the more conventional transmissions and typical coastdown results. The final results suggested that this research could aid in separating transmission losses from a vehicle's road load derived from a coastdown test. This would leave only the drag coefficient term and rolling resistance.

At this time there are not many other true vehicle coastdown works past 2020. Other studies have been done on road load prediction through regression modeling [52]. But these studies do not perform a full coastdown experiment. Another loss study by Shore et al. found that EV gearboxes can account for 13 - 25% of the powertrain losses compared to only 6.5% in a conventional ICE transmission [53]. However, again, this is not a full vehicle coastdown study.

3. Methodology and Test Procedure

All testing methodologies and procedures outlined below are derived and slightly modified from SAE J1623 [54], SAE J2263 [38], Intertek [25], and ETA-HITP01 [55]. The modifications are due to vehicle type, testing location/allowed use of facilities at the track, and measurement capabilities.

3.1 Coastdown Conditions, Test Location, and Weather

This research explored 4 different coastdown conditions using the same 2019 Chevy Blazer HEV. All 4 conditions disconnected the vehicle's 9-speed transmission via the clutch between the engine and transmission. The 4 procedures are outlined below and detail the conditions of the electric drive unit (EDU). Conditions III and IV featured two methods for post-processing the force due to the EDU previously outlined in Equations (4) and (5).

I. Standard operating condition/typical coastdown conditions/control (TCC)
    a. EDU clutch disconnected
    b. 0 Nm wheel torque commanded
II. EDU contribution test 1 (ECT1)
    a. EDU clutch connected
    b. 0 Nm wheel torque commanded
III. EDU contribution test 2 (ECT2)
    a. EDU clutch connected
    b. Constant 200 Nm regen wheel torque commanded
IV. EDU contribution test 3 (ECT3)
    a. EDU clutch connected
    b. Constant 400 Nm regen wheel torque commanded

TCC was regarded as the control and baseline for the WVU Blazer for this research. Since coastdown results can vary because of track conditions and weight, it was important to establish a baseline road load for this vehicle, on this track, and at this weight to compare other coastdown conditions to. It was also important to establish a baseline for this vehicle as it is a student designed prototype vehicle with no defined road load coefficients to base this research's results off of. ECT1 was the secondary baseline test for this research. The purpose of establishing a secondary baseline was to recognize any effects that the EDU's spin loss has on the vehicle's road load and how this road load compares to ECT1. For ECT2 and ECT3 the negative torque command was chosen through calibration and driver comfort at speeds above 60 mph. All 4 conditions featured 9 complete coastdown tests with 2 runs in both directions in a modified manner following [25]. To minimize the number of data files, each set of runs (down and back) are on one log file. All testing occurred at the Transportation Research Center (TRC) just outside of East Liberty, Ohio northwest of Columbus, Ohio. Testing occurred at TRC's large oval circuit with 2.25-mile straightaways and 1.4 miles of dedicated lane space for this testing. On their large oval track, only one direction of travel is allowed. Contrary to most coastdown tests, the opposing runs were performed on the opposing runways as shown in Figure 4 by arrows 1 and 2. This is due to the rules around shared use of the large oval track.

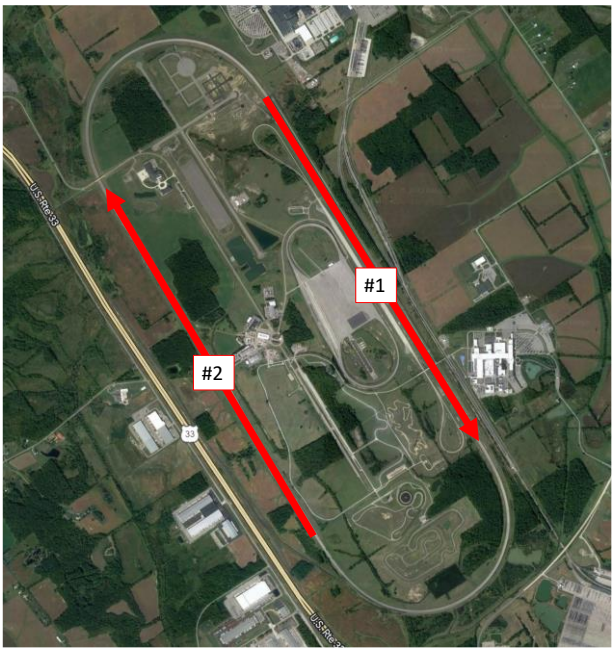

Figure 4: Opposing coastdown tests at TRC

The two corners at the northwest and southeast corner of the track were used to gain vehicle velocity to a value at or above 75 mph and stabilize at that speed for the duration of the corner before coasting occurs. These two corners were also used to stabilize the battery's SOC before the two coastdown conditions in which the EDU clutch is engaged, and the controller is commanding negative motor torque. It is important to note that all lanes at TRC have different speed limits, both a minimum speed and a maximum speed with a 10-15 second limit on stopping time allowed.

For all run 1 tests, the track sloped slightly downhill with approximately a 0.13% grade. For run 2s, an uphill grade of 0.27% was observed. To accurately compare data from both runs, the force acting on the vehicle due to grade was removed from each respective run's force term. This process is shown in a later section in more detail.

3.1.1 Weather Conditions

The weather conditions for the testing date for East Liberty, Ohio are shown below in Figure 5. The green box represents the time the vehicle was actively on the track. The TRC track-specific wind

conditions are shown after in Table 2 and Figure 6 respectively. The goal behind understanding the wind speed was to remove any force due to wind contribution to the road load of the vehicle from each run.

Figure 5: East Liberty, Ohio general weather conditions on the testing day [56]

Table 2: Wind speed and direction taken in 30 minute increments at the West VDA pad at TRC

Time	Wind Speed (mph)	Direction
8:00:00 AM	7	SW
8:30:00 AM	9	SW
9:00:00 AM	9	SSW
9:30:00 AM	8	SSW
10:00:00 AM	11	SW
10:30:00 AM	14	SW
11:00:00 AM	5	SW
11:30:00 AM	6	SW
12:00:00 PM	15	S
12:30:00 PM	13	SW
1:00:00 PM	11	S
1:30:00 PM	9	SSW
2:00:00 PM	6	S
2:30:00 PM	14	SSE
3:00:00 PM	9	S
3:30:00 PM	11	SSE
4:00:00 PM	17	SSW

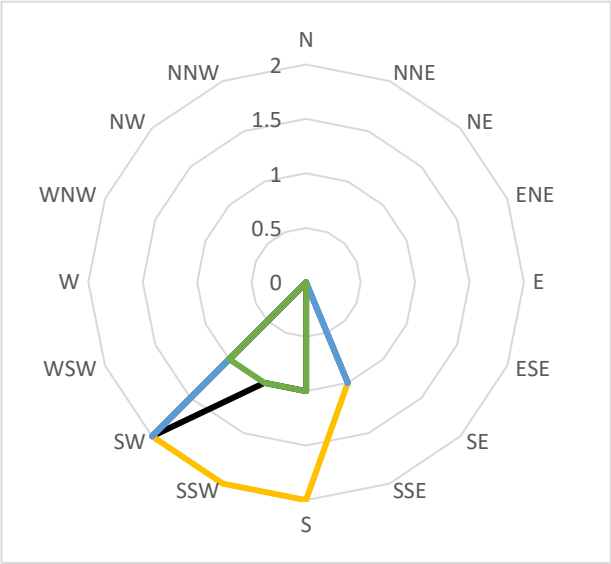

Figure 6: Wind rose for occurrences of wind speed and direction at TRC on April 29th, 2023

The average speed of the wind on the day of testing was 10.24 mph with a standard deviation of 3.35 mph. The average direction of the wind was from the SSW direction and was roughly 21.2° from S. This

is not exactly perpendicular to TRC which means that wind contribution cannot be assumed zero. The average measured wind speed in the longitudinal direction for run 1 was a 3.1 mph headwind and for run 2 it was a 3.6 mph tailwind. The average air temperature for the testing day was 59 °F and there was no precipitation. The relative humidity which is not shown in Figure 5 was an average of 70% during the testing period. The barometric pressure was on average 28.84 inHg through the day as well [56]. The final force due to wind contribution will be computed in a later section.

3.2 Testing Materials and Vehicle Weight

I. Two EcoCAR team laptops with chargers
    a. One for dSPACE Control Desk to interface with the vehicle's controller
        i. Control Desk is used to change modes of operation to modify the vehicle's controller in real time to perform each test
    b. One for Vector CANoe for all CAN logging troubleshooting that might be needed.
II. The EcoCAR Vector CAN logger model: VN1630 log
    a. Measures up to 4 CAN channels
III. Anemometer for wind speed measurements
IV. Tire pressure measurement device

The vehicle used for all testing has been described previously as a student-led competition prototype HEV 2019 Chevy Blazer. The vehicle has a dry mass of 1955 kg and an experimental mass of 2182 kg. It was assumed that for all testing, the mass of the fuel was constant. Each tire was filled to the factory recommended 36 psi and the experiments began with a full tank of fuel. It was also assumed that tire pressure was constant for the day of testing.

3.3 Coastdown Test Procedure

I. Before each run, the copilot placed the controller in the correct state using Control Desk to change the calibratable parameter associated with the specific condition to be tested.
    a. Due to the track size, once the controller was set into the proper condition, the vehicle was then “switched back” to normal operation using a failsafe calibratable to ensure the ECMS algorithm could properly balance the battery’s SOC.

II. The order of testing followed the order that the conditions are presented to ensure each condition was tested under similar conditions for each test and run.
    a. The order was as follows: TCC, ECT1, ECT2, ECT3

III. After selecting the proper test through the calibratable parameter, the driver entered the vehicle into one of the two corners.

IV. During the corner, the vehicle speed must increase to 75 mph or above and stabilize prior to the straightaway. Approximately ¾ of the way through the corner, the copilot disengaged the failsafe calibratable and revert the vehicle back into the testing state described earlier.

V. As the driver exited the corner, they merged into the dedicated coastdown lane to begin testing.

VI. The driver then straightened the vehicle in the center of the lane and shifted the vehicle into neutral beginning the official coastdown.
    a. At this time the copilot confirmed that the EDU’s clutch was in the correct state and the test continued or abort.

VII. If the clutch was in the proper state, the driver coasted the vehicle to below 10 mph or until the dedicated lane ended.

VIII. The driver brought the vehicle to a complete stop and recorded the wind speed before returning to the first step.

a. The copilot also recorded any potential standard issues as well as the wind speed in a log table.

IX. At this point, this specific coastdown ended and the steps repeated.

3.4 Summary of Collected Data

As mentioned previously the WVU Chevy Blazer's CAN signals were logged using the Vector VN1630 log logger. This logger monitored the traffic on 4 CAN channels in the Blazer. The first channel was the gatewayed GM highspeed (HS) channel which contained all GM stock vehicle signals that the team-added controllers monitored and used for decision-making purposes. The second CAN channel was the controller's communication with the team-added battery. On this channel, the battery's status was accessible and monitorable. The third CAN channel was the primary control bus. All of the controller's commands were sent through this bus to the vehicle's transmission, engine, and EDU. The last channel was the chassis expansion channel where the signals to and from the electronic brake control module (EBCM) reside. Due to AVTC and GM NDAs, the exact signal names can't be mentioned. However, for this thesis Table 3 below lists the primary logged signals used for the data reduction and analysis.

Table 3: List of Logged Signals Used For Data Reduction

Signal	Units	CAN channel
Vehicle Speed	Kilometers per Hour	Channel 1
Brake Pedal Position	Percentage	Channel 1
HV Battery Voltage	Volts	Channel 2
HV Battery Current	Amperes	Channel 2
EDU Speed	Radians per Second	Channel 3
ECU Torque (in-wheel torque)	Newton-meter	Channel 3

This work did not need to use channel 4 as the EBCM is only commanded by the controller during ACC or hill stops. The six signals presented in Table 3 were out of 42 of the signals that the AVTC competition rules dictated the vehicle's logger must capture. The true number of signals logged in is much higher than this but cannot be disclosed due to NDAs. Below, examples of raw, trimmed data are shown for all 4 test conditions.

3.5 Generalized Data Reduction Methodology

While each coastdown condition has varied methods of data reduction that are discussed shortly, the methods in this section were used by all four conditions. This assumed methodology aided in consistent results derivation.

3.5.1 Data Conversion

Each log file contained on the Vector logger were formatted as a binary logger file (BLF). A BLF is a CAN message-based file type that is used primarily by Vector. The message packaging utilizes a set of DataBase Container (DBC) files (one file per CAN channel) which help the BLFs organize the message

structure for each packet. Within specific message packets within each BLF file are the logged signals needed for this testing according to Table 3. BLF files were useful when plotting and analyzing data with Vector software, however, they needed to be converted to a friendlier file format for further analysis. The first necessary item to complete with each log file contained on the SD card in the logger was to convert the BLF to a comma-separated value (CSV) file type. The VN1630 log does not support direct conversion to MATLAB files (MAT). After converting the BLF to a CSV file type using the blfread command in MATLAB [57], the log file was trimmed further for size purposes to only contain the 42 AVTC-required signals. Once the file was trimmed appropriately and renamed to the appropriate test and or condition then the file was ready for further post-processing.

3.5.2 Final Data Trimming

The first step in further post-processing was to eliminate unnecessary portions of each coastdown using a data trimming tool developed by Sam Reinsel of MathWorks for the final year of the EMC to aid the competition teams in quickly analyzing data and developing their post-processing scripts. This tool was embedded within a MATLAB app and it produced a visual of the data trimming process and the user could select one or more windows to cut their data down to. An example of the trimming tool is shown below in Figure 7.

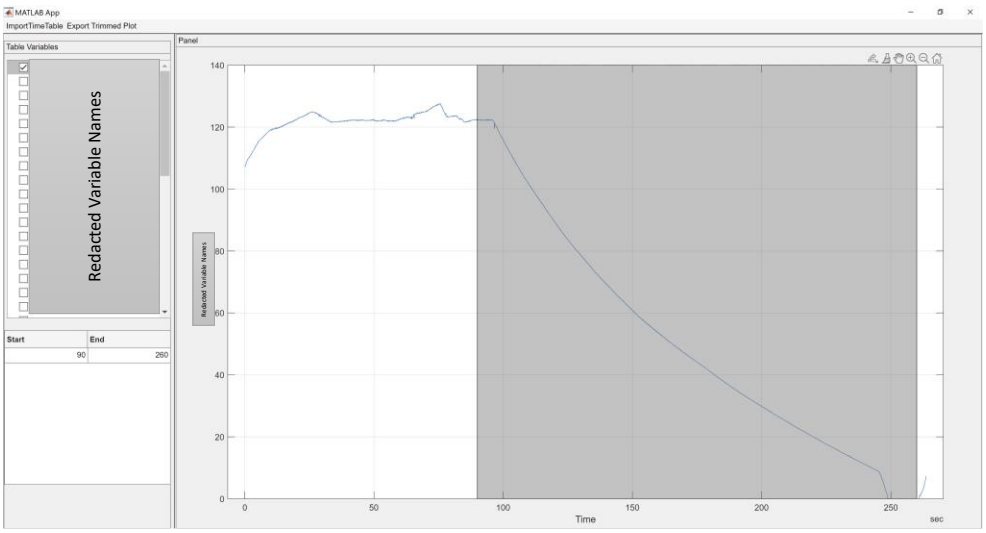

Figure 7: Data trimming tool using the velocity from TCC test 1 run 1

As shown, each coastdown was trimmed from seconds before the gear lever was placed into its neutral state to seconds after the vehicle slowed to a full stop through the driver applied brakes. After the files were trimmed and sorted with the above method, they were fed through a post-processing script where the final data trim occurred.

The final data trimming was the same for each coastdown condition and occurred at the beginning of the post-processing script. The post processing script would find the index where the vehicle speed would first dip below the starting speed threshold and define that velocity as the new starting velocity. For each coastdown a consistent initial vehicle speed of 31.5 m/s (~70 mph) was chosen. The shift to neutral occurred for each coastdown at varied vehicle speeds between 77 and 74 mph after the driver stabilized the vehicle and began the merging process into the dedicated coastdown lane at TRC. Choosing an initial velocity of 70 mph ensured that the vehicle speed was firmly in its second-order descent towards 0 mph. The ending point of each test was chosen as the point at which the vehicle's brake pedal was depressed by more than 1.5%. The value of 1.5% was chosen as it was approximately double the steady state unpressed value of the pedal which was approximately 0.75%. The instant the brake pedal was pressed and exceeded the defined threshold, that particular coastdown test would end

and the data trimming was complete. For run 1s, the average ending speed was higher than the average ending speed of run 2s due to the road grade at TRC.

3.5.3 Vehicle Acceleration Determination and Smoothing

The steps to obtain the trimmed velocity were only the first steps in the data reduction process in obtaining the road load for each coastdown condition and each individual run. The next step in the data reduction process used for each condition was determining the acceleration $\dot{v}$ from a derivation of the velocity collected during the coastdown event as shown in Equation (6).

$$\dot{v} = \frac{\Delta v}{\Delta t} \tag{6}$$

Where Δv represents the difference in vehicle velocity for a single time step and Δt represents that time step. It was observed that the initial acceleration term from the first round of derivations was quite noisy. This noise and the magnitude of the acceleration peaks indicated discontinuities in the velocity vectors due to the logging timestep. To mitigate these discontinuities, each velocity vector was smoothed using a Savitzky-Golay filter implemented through the MATLAB smooth function. The version of MATLAB's Savitzky-Golay filter used to filter and smooth the velocity curve used a least-squares fit of a 2nd-order polynomial. This polynomial was then fit over the velocity's values through a rolling window and the central point of this polynomial within the window was the new data point [58][59]. The rolling window size chosen for data reduction and analysis was 2 seconds (1 second on either side of the centroid). The 2 second window size was chosen through trial and error. Too large of a window caused discontinuities with the calculated acceleration and too small of a window eliminated the positive effects of the filter. The difference that the Savitzky-Golay filter makes on the velocity and acceleration curves is shown below in Figure 8 and Figure 9.

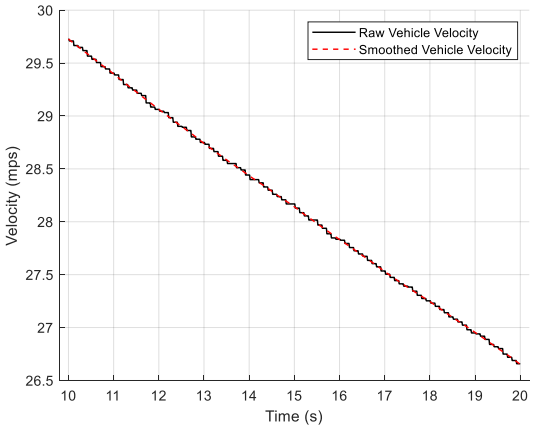

Figure 8: Raw vehicle velocity versus smoothed vehicle velocity over a 10-second timeframe

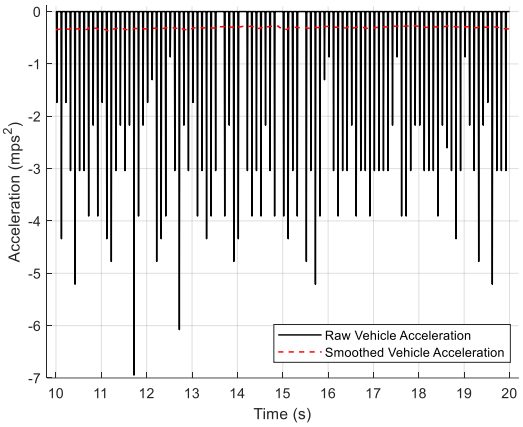

Figure 9: Raw vehicle acceleration versus acceleration derived from smoothed vehicle velocity over the same 10-second timeframe

While the smoothing had a minimal effect on the velocity, it did remove the step-change aspect of the raw signal enabling a cleaner differentiation to obtain a manageable vehicle acceleration. This "step-like" behavior of the velocity caused the large magnitudes in acceleration changes followed by zero acceleration events as the velocity was constant for that segment of time. The Savitzky-Golay filter smoothing with the same 2-second rolling time was then applied to all coastdown conditions and all runs within each coastdown condition. For each condition, the acceleration was observed and it was ensured that no modifications to the filter style or rolling window size were needed.

3.5.3 Grade Contribution Removal

For an ideal coastdown, the section of roadway used for each coastdown would be perfectly flat and straight. Unfortunately, this type of roadway is difficult to produce east of the Mississippi River due to the rolling hills and mountains. TRC is the closest facility to WVU which provides the longest straightway at a minimal grade. The reasoning behind this analysis is the test vehicle would roll significantly further during the TCC and ECT1 run 1s with a higher final vehicle speed than the run 2s. It was noted that the grade of each straightaway would need to be calculated and then the contributing force due to that

grade would need to be removed from the resulting road load equation for each coastdown condition. Although the grade is minimal, each straightaway at TRC has a different grade and cannot be assumed to be 0%. The grade mentioned previously was 0.13% downhill for all run 1s and 0.27% uphill for all run 2s and was calculated through a rise-over run methodology. For example, a rise of 1 meter over 100 meters is a 1% uphill grade. In order to properly compare and contrast the coastdown results using runs from both straightaways at TRC, the force contribution due to grade needs to be removed. The force due to grade is the third term in Equation (3). The angle α is determined through the inverse tangent of the grade (rise over run of a right triangle) as shown in Equation (7).

$$\alpha = \tan^{-1}\frac{rise}{run} \tag{7}$$

Both the rise and run were determined through Google Earth which does have some uncertainty, but not high enough to prevent the assumptions for the grade based on the values derived from their system [60]. For ease of understanding, this thesis presents the angle α in degrees, but for all calculations, it was converted to radians. The mass m is the vehicle's mass defined previously and g is the acceleration due to gravity assumed to be 9.81 $\frac{m}{s^2}$. The direction in which the force due to the road grade acts is determined by the direction of the slope in the road. For example, the force due to grade is acting against the vehicle if the slope of the road is positive as shown in Figure 2. To remove the contribution of road grade from the coastdown results, the force due to grade must be added to a downhill coastdown run and subtracted from an uphill coastdown run. The final contributions and whether the terms were added or subtracted from the road load for each run at TRC are shown below in Table 4.

Table 4: Force due to road grade summarization table

	TRC run 1	TRC run 2
Grade (%)	0.13	0.27
Angle α (degrees)	0.075	0.155
Force F_G (N) (defined in Equation (3))	27.83	57.91
Addition or Subtraction	Addition	Subtraction

The force due to the road grade's contribution was then removed from each coastdown dependent on the run. The grade's influence in the testing did factor into the final vehicle speed capabilities for each respective run. For run 1s, the final vehicle speed would only reach 12-18 mph or before the driver would apply the brakes to end the test. For the run 2s, the vehicle would reach a much lower speed consistently (~8 mph) before the driver would apply the brakes to end the test.

3.5.4 Wind Contribution Removal

The final factor accounted for in this coastdown testing is the force contribution on the test vehicle due to the wind speed at TRC the day of testing. The average wind speed and direction were found earlier from the data collected by TRC shown in Table 2. For this research, the contribution of wind in the direction perpendicular to the direction of the vehicle's forward motion were omitted. This contribution was omitted as the test vehicle does not have the sensor suite capable of measure the transverse effect of wind. In order to understand the contribution of the force due to wind speed, it is first necessary to understand how much of the wind is actually contributing in the direction of forward motion of the test vehicle. It is known that the average wind speed on the day of testing was 10.24 mph from the SSW direction and 21.2° from S. Based on the estimations drawn from Google Earth analysis and represented by Figure 10 with the red arrow, the angle between the wind and the test track straightaways is roughly

55°. Through basic trigonometric functions, this means that the wind acting along the direction of the test track is 5.8 mph and is represented by the green arrow.

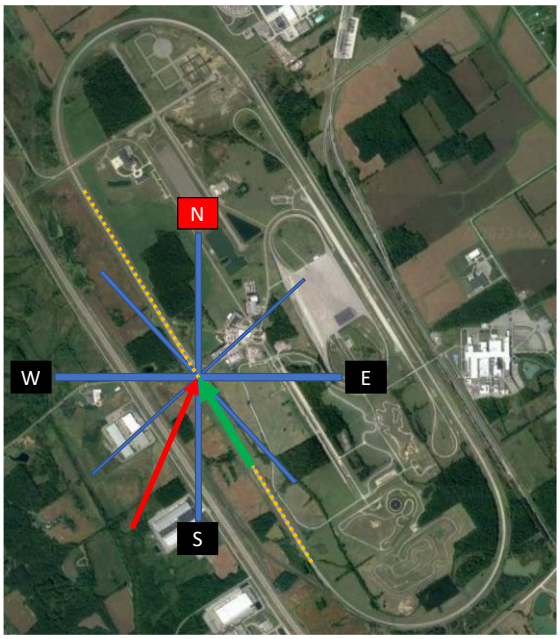

Figure 10: Compass overlayed with the pit lane of TRC showing average wind direction relative to the track

The 5.8 mph wind speed acting along the length of the test track is not the wind speed used in the final calculation of the contribution. The final acting wind speed is an average of the wind speed calculated and the two wind speeds (3.1 and 3.16 mph) which were averages of the collected wind speed from the day of testing on each run. Each of the measured wind speeds were collected at the end of each respective run. The run 1 collected wind speed was a headwind and the run 2 collected wind speed was a tailwind. The TRC measured wind speed was collected in the middle of the TRC compound. The average of these three wind speeds is 4.17 mph. SAE J2263 defines the drag due to the aero effects of the vehicle during the coastdown as shown below in Figure 11.

11.4 Aerodynamic Drag Modeling—The aerodynamic drag coefficient, $C_d(Y)$, is modeled as a four-term polynomial with respect to Yaw angle (Y, Deg) (see Equation 3):

$$C_d(Y) = a_0 + a_1 Y + a_2 Y^2 + a_3 Y^3 + a_4 Y^4 \quad \text{(Eq. 3)}$$

where:

a_0 to a_4 are constant coefficients whose values are determined in the data analysis. The aerodynamic drag coefficient is combined with the vehicle frontal area (A) and relative wind velocity (V_r) to determine the aerodynamic drag (D_{aero}). See Equations 4 and 5.

$$D_{aero} = (1/2)\rho A V_r^2 C_d(Y) \quad \text{(Eq. 4)}$$

$$D_{aero} = (1/2)\rho A V_r^2 (a_0 + a_1 Y + a_2 Y^2 + a_3 Y^3 + a_4 Y^4) \quad \text{(Eq. 5)}$$

Figure 11: SAE J2263 section 11.4 describing how the SAE recommends modeling aerodynamic drag[38]

The SAE's recommendation reflects the use of an onboard anemometer to accurately find the relative wind velocity for the drag contribution of the road load. Because this research does not have this relative velocity built into the drag term of the final tractive force equation, a different approach is needed to determine the accounting method for the force due to wind speed. To find the force due to the wind speed, the drag force due to the nominal vehicle speed and the drag force due to the relative vehicle velocity (assuming a constant wind speed of 4.17 mph) were compared. The difference between the two drag forces is the force due to the wind speed the day of testing and Equation (8) below represents this calculation.

$$F_{wind} = \frac{1}{2} C_d \rho A ({V_{relative}}^2 - V^2) \quad (8)$$

The term $V_{relative}$ represents the relative velocity of the vehicle with respect to the wind speed and direction. For all run 1s, the relative velocity of the vehicle is slower than the nominal velocity due to the headwind during testing. For all run 2s, it is faster due to the tailwind. The vehicle's nominal velocity is represented by *V.* The coefficient of drag for the 2019 Chevy Blazer is approximated as 0.35 [61] and the frontal area is calculated as 2.65 m^2 through the methods in [29]. From the weather conditions

described earlier, the average air density on the day of testing is 1.1753 $\frac{kg}{m^3}$. With all parameters now known, an example of the force due to wind contribution is displayed below in Figure 12.

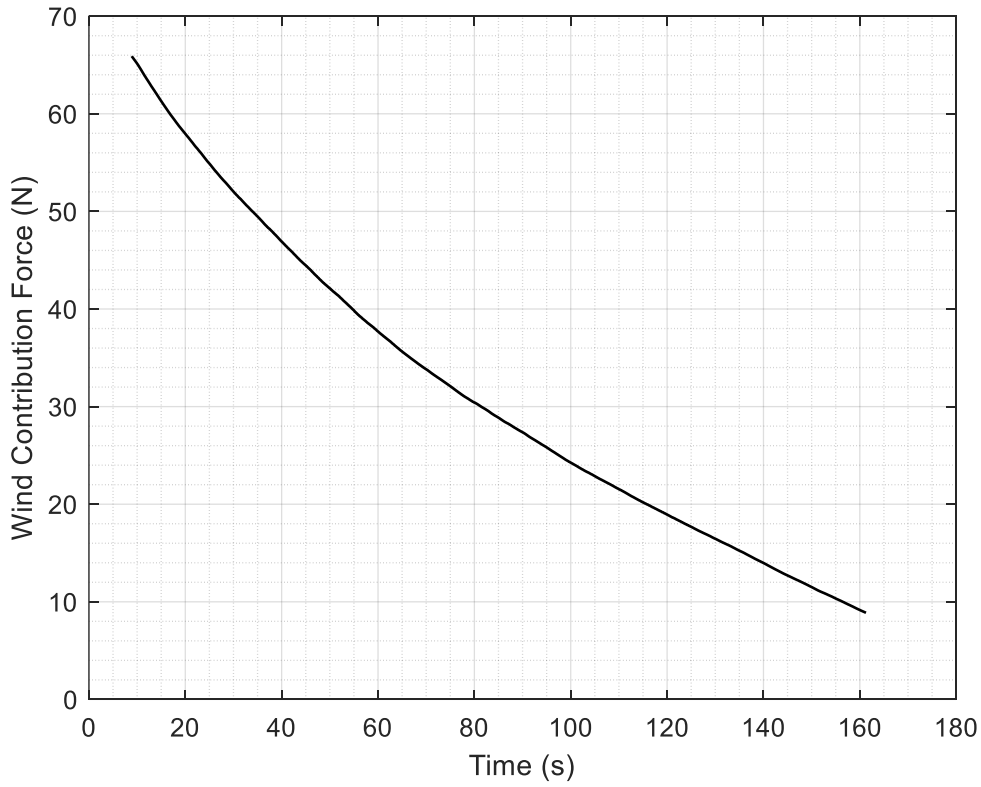

Figure 12: Representation of the force due to the wind contribution for a TCC Run 2

The force is a second order polynomial that decreases as vehicle speed decreases which is expected based on the literature review of this research. This force due to the wind speed contribution was removed from each coastdown run, using this methodology, for all 4 coastdown conditions.

3.6 TCC and ECT1 Specific Methodology

The Typical Coastdown Conditions (TCC) data set is the control set for the Blazer where the EDU clutch and the vehicle's clutch are disengaged and the standard coastdown procedure is followed. The EDU Contribution Test 1 (ECT1) data set is the secondary "control" test. The ECT1 condition keeps the EDU clutch engaged with no torque commanded and the vehicle's transmission in neutral. Ideally, ECT1

would demonstrate the spin losses associated with the EDU engagement versus the standard coastdown conditions of the TCC. For each TCC and ECT1 run, only the Vehicle Speed, and Brake Pedal Position are needed for data reduction purposes. Following the trimming and methods described previously, the next steps for the TCC and ECT1 conditions are to compute the grade and wind-adjusted road load for each run. The grade adjustment was defined previously and does not change for each coastdown condition but does change sign and magnitude dependent on which straightway the run was performed on (run 1 or run 2). Please refer back to Table 4 for the sign and magnitude of the force due to road grade. The wind adjustment was also performed previously and the force is displayed in **Error! Reference source not found.**. The direction of this force also changes depending on which run is being analyzed. The grade and wind-adjusted road load is calculated through Equation (9) below which is modified from Equation (1) to include the force due to grade and the force due to wind. The absolute value is to ensure that the resultant force is positively acting on the vehicle. Because of the negative acceleration term for the duration of the experiment, this is necessary.

$$F_t = |m_v \dot{v}| \pm F_G \pm F_{wind} \tag{9}$$

Where F_t is the tractive force which for Equation (9) it is also representative of the resistive force. The mass of the vehicle multiplied by the acceleration is represented by $|m_v \dot{v}|$. F_G is the grade contribution and F_{wind} is the wind contribution. At this point each individual coastdown run for the TCC and ECT1 conditions are now complete and ready for further analysis and discussion.

3.7 ECT2 and ECT3 Specific Methodology

The two EDU contribution tests which have the EDU clutch engaged and negative torque output from the EDU are ECT2 and ECT3. This is comparison to ECT1 which has a torque command of 0 Nm. The only difference between the two conditions is the amount of negative torque. ECT2 with -200 Nm and ECT3

with -400 Nm. For each of these two conditions there are two methods of eliminating the negative torque contribution to the force acting on the vehicle during the coastdown event. The first of the two methods are outlined previously by Equation (4). It is important to eliminate the contribution of the negative torque command as it is an additional drag force that contributes to a higher overall road load for these two conditions. The methods outlined below are useful if performing a coastdown on a vehicle that cannot be placed into a true neutral state.

3.7.1 Force Contribution Derived from Measured Torque

In order to implement Equation (4) into Equation (9), more of the standard logged signals need factored into the post-processing scripts. The two additional signals needed as prescribed by [25] are the motor's torque at the wheels in Nm and the motor's speed in radians per second. The only modification needed for this condition to implement Equation (4) is the conversion of motor speed from rpm to radians per second. With this conversion finished, Equation (10) is formed below to compute the road load accounting for and eliminating the contributions of grade, wind, and back EMF forces through the EDU torque and speed methods.

$$F_t = |m_v\dot{v}| \pm F_G \pm F_{windconst}\text{-}F_{backEMFts} \quad (10)$$

All terms of Equation (10) are the same as (9) with the addition of the back EMF force contribution. The second method is described earlier by Equation (5) and is outlined next.

3.7.2 Force Contribution Derived from Battery Power

The second methodology outlined in [25] is suggested for researchers who are unable to monitor torque and speed information for their EDU but can monitor HV battery signals. Fortunately, the vehicle used for this testing monitors all of the above. To use Equation (5), it is first required to compute the battery power P_{batt} used for the duration of the coastdown test. From Ohm's Law, it is known that power equals

the product of voltage and current. Then when that power is divided by a vehicle speed, the back EMF force is calculated. After the force is calculated specific to the battery power, Equation (11) is formed below to compute the road load accounting for and eliminating the contributions of grade, wind, and back EMF forces through the EDU HV battery power method.

$$F_t = |m_v\dot{v}| \pm F_G \pm F_{windconst}\text{-}F_{backEMFp} \quad (11)$$

All terms of Equation (11) are the same as (9) with the addition of the back EMF force contribution.

3.8 Curve Fitting Road Loads

The Savitzky-Golay filter mitigated most of the noisiness in the calculated vehicle acceleration. However, the resultant road load curves for each coastdown conditions calculated via Equations (9), (10), and (11) with respect to velocity were still quite noisy. Even with the noisiness, there is still a clear and apparent second-order behavior to each curve. With one of the primary goals of this research centered around comparison of the four different coastdown conditions, it was necessary to perform polynomial curve fitting with each individual coastdown test to obtain comparable coefficients of each polynomial. These comparable coefficients are the "A", "B", and "C" values often published by the EPA or other researchers. To obtain the comparable road load coefficients for further analysis, MATLAB's built-in functions were used. The two functions are polyfit [62] and polyval [63]. For this research, polyfit was used to automatically return the 3 coefficients of a second-degree polynomial for each individual coastdown test. The other function, polyval, was utilized for understanding the quality of the curve fits and producing a plottable trace of the three coefficients output by polyfit. The plottable collective fit trace and the average of the three coefficients was found for each of the coastdown conditions. The collective fit for all tests for one coastdown condition was compared to the collective fit for the other coastdown conditions to analyze.

4. Results and Discussion

This section outlines the results of all four coastdown conditions; TCC, ECT1, ECT2, and ECT3 in that order. Each coastdown condition's cumulative and comparable coefficients will be outlined. This also includes a predicted error band for the finalized curve and coefficients. For ECT2 and ECT3 an additional comparison will be outlined between the two different methodologies to eliminate the back EMF force contribution. The comparison between the four coastdown conditions is the final portion of this section along with a discussion about the feasibility and capability of the test methodology used. Part of this comparison includes discussion on the differences between the two methods of accounting for the back EMF force contribution in the EDU. A statement will also be made (if the logging capabilities are there) on which method of accounting for the back EMF force contribution is better.

4.1 Control Conditions Results

The two control conditions this thesis explores are the TCC and ECT1 conditions. As a reminder, the TCC conditions are as close as possible to a traditional coastdown conditions with both the EDU and the vehicle's transmission disengaged. The ECT1 condition is the same as the TCC conditions except the EDU clutch is engaged to see if there is a contribution of rolling resistance from the rotating portions of the DU that will offset the results discussed for the ECT2 and ECT3 conditions.

4.1.1 TCC Results

The TCC coastdown condition is the control test to which the other three conditions will be compared. Using methods described previously, a polynomial curve fit is applied to each individual coastdown test and then those curve fits are compared to determine a final cumulative curve fit. All 18 coastdown tests along with the best fit curve for all 18 are shown in Figure 13. The polynomial curve fit coefficients of the average tractive force at each velocity of the 18 coastdowns are shown in Table 5.

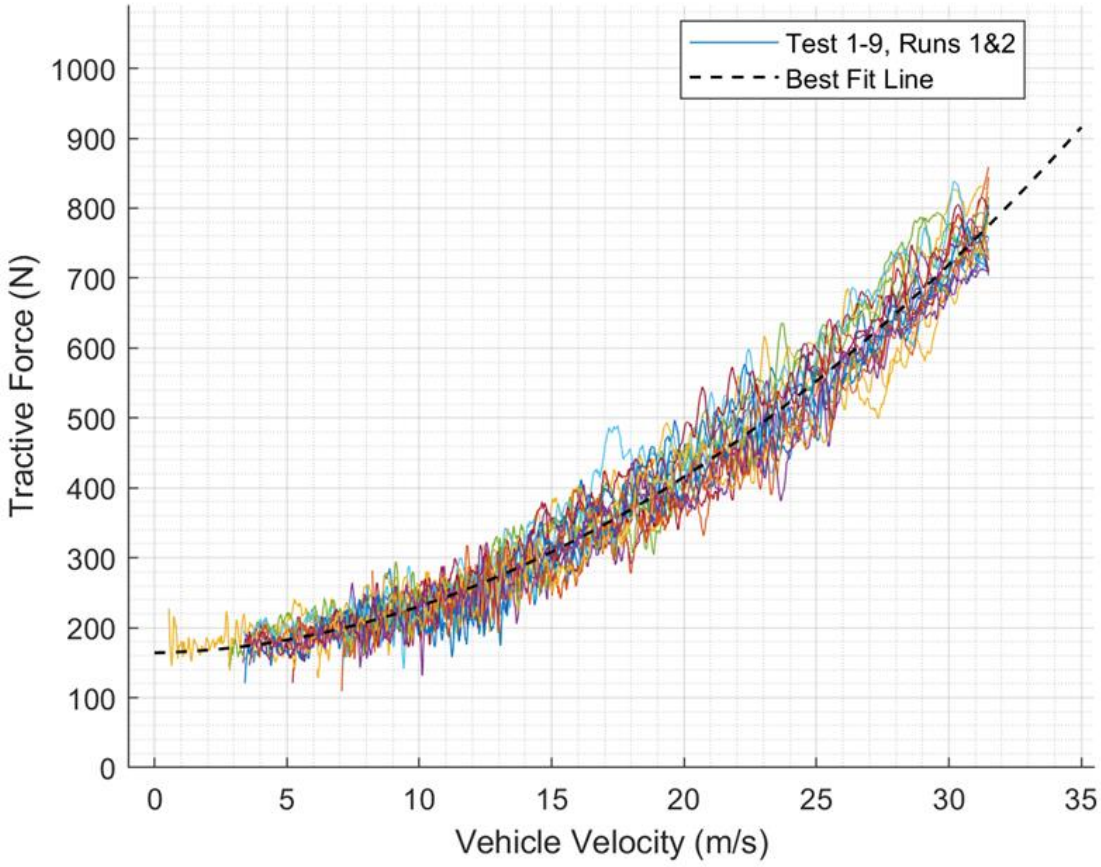

Figure 13: TCC results for the 18 coastdowns with the best fit line overlayed

Table 5: TCC 3-component road load constants 'A', 'B', and 'C' results from the 18 coastdowns

A (N)	B $(\frac{N}{m/s})$	C $(\frac{N}{m^2/s^2})$
157.09	1.674	0.569

What appears to be a visually large fluctuation in calculated tractive force shown in Figure 13 leads to another methodology to understand the results for the ultimate goal of comparing the different coastdown methodologies. Using the polynomial curve fits derived from each individual coastdown above, the ideal tractive force at each vehicle speed was calculated for each of the 18 coastdowns and a box and whisker chart was created below in Figure 14. The box and whisker plot was used as it shows

the overall spread of the tractive force at each vehicle speed as well as provides a region where one could expect the majority of test results to lie in order to be statistically significant.

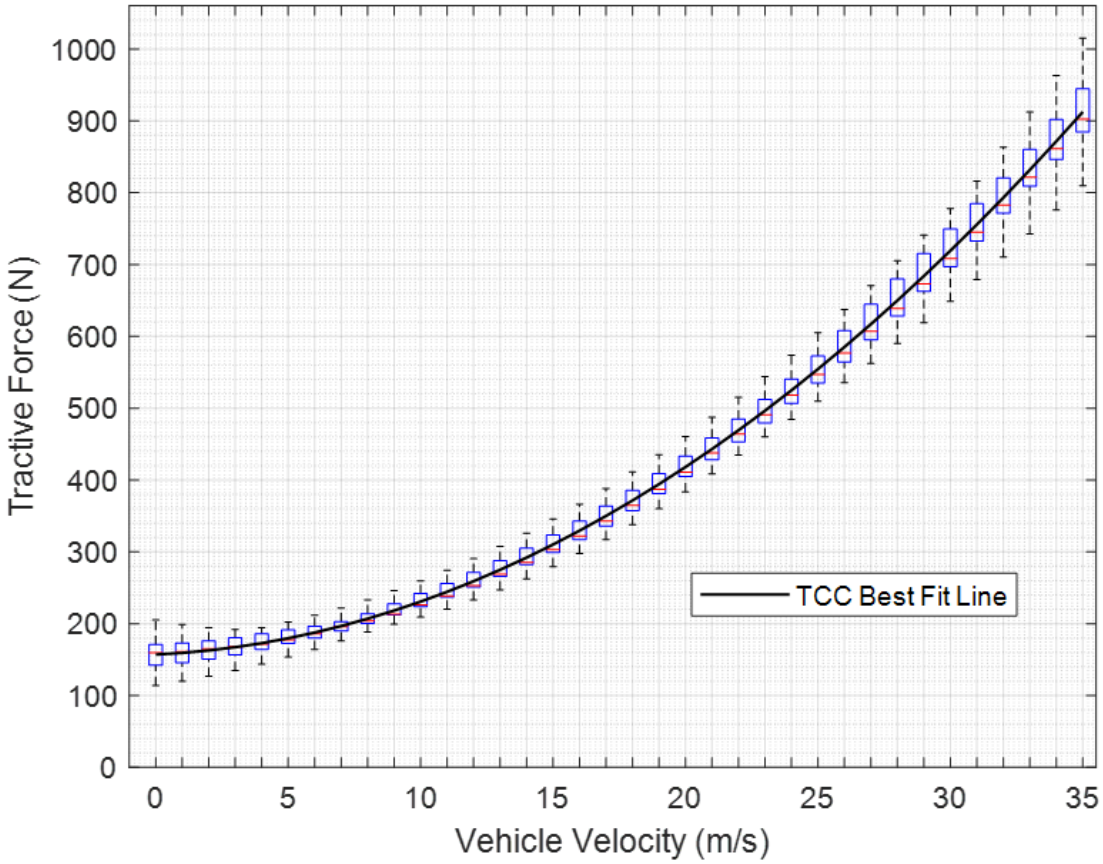

Figure 14: Box and Whisker Plot of the Calculated Tractive force from 0 to 35 m/s for the TCC coastdown condition with outliers removed

Due to one of the nature of full vehicle testing, there was one outlier for the 18 total coastdowns within the TCC condition. Test 5 Run 1 was removed from the results as it was a large outlier in comparison to all other tests and runs and showed much higher tractive forces at low vehicle speed. This outlier was over 3 standard deviations and 4.68 interquartile ranges from the median therefore it was removed from the dataset. The best region with the lowest overall spread of tractive force is relatively large and is roughly from 3 m/s to 25 m/s. This is expected as the regions above 25 m/s are mostly dominated by coefficient of drag forces and regions below 5 m/s are typically dominated by rolling resistance forces.

The road load constants for all tests and conditions do not change between the results and the box and whisker plots. Overall, the TCC results serve as a viable baseline to compare the ECT1 results to and form conclusions about the overall data.

4.1.2 ECT1 Results

Similar to the TCC condition, 18 coastdowns were performed and a final polynomial curve fit was calculated from the fit of each individual coastdown. All 18 coastdowns along with the best fit line are shown in Figure 15. The resulting A, B, and C values from the polynomial curve fit of the average tractive force values at each vehicle speed for the ECT1 results are shown in Table 6.

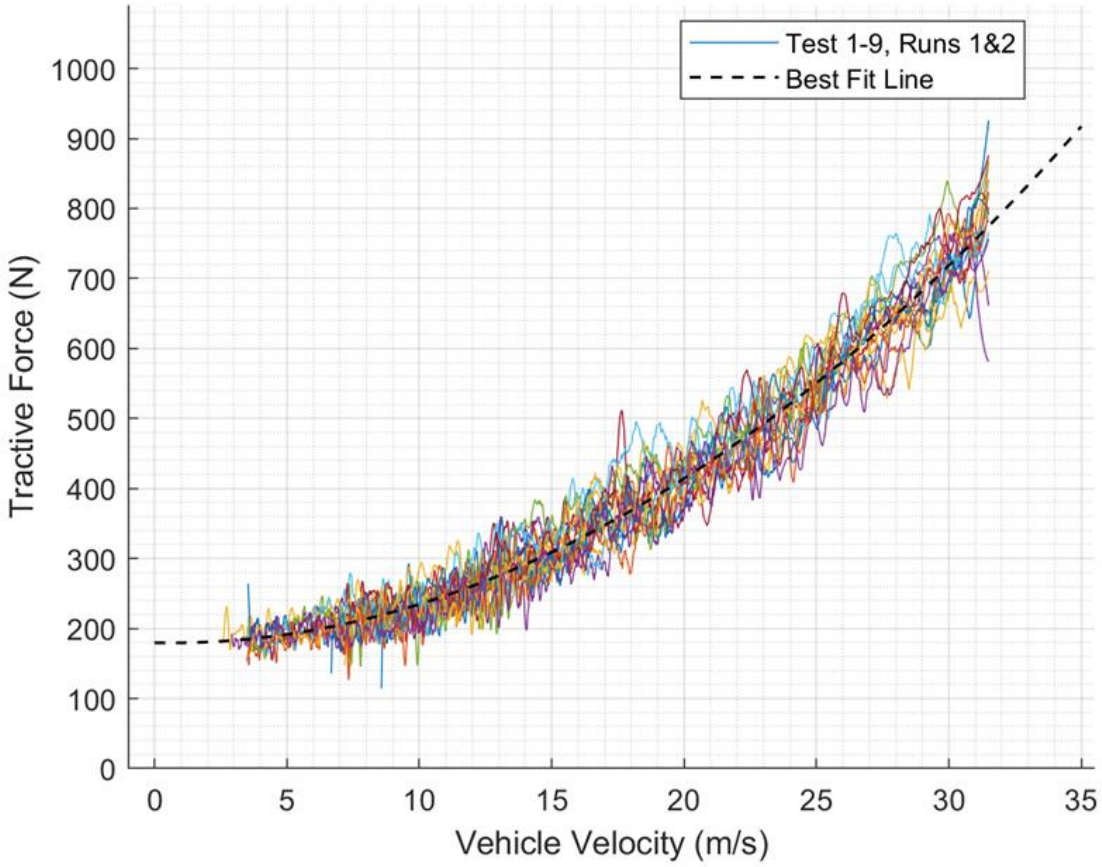

Figure 15: ECT1 results for the 18 coastdowns with the best fit line overlayed

Table 6: ECT1 3-component road load constants 'A', 'B', and 'C' results from the 18 coastdowns

A (N)	B $(\frac{N}{m/s})$	C $(\frac{N}{m^2/s^2})$
183.93	-1.205	0.635

The same methodology used to expand the TCC results with a box and whisker plot are used here for the ECT1 results as well shown below in Figure 16. One outlier was removed from the results as it showed a considerably lower tractive force at vehicle speeds below 5 m/s which did not match the expected results of the other 17 coastdowns. This outlier was over 2.5 standard deviations and 2.1 interquartile ranges from the median. Test 5 Run 1 was the outlier removed from the results.

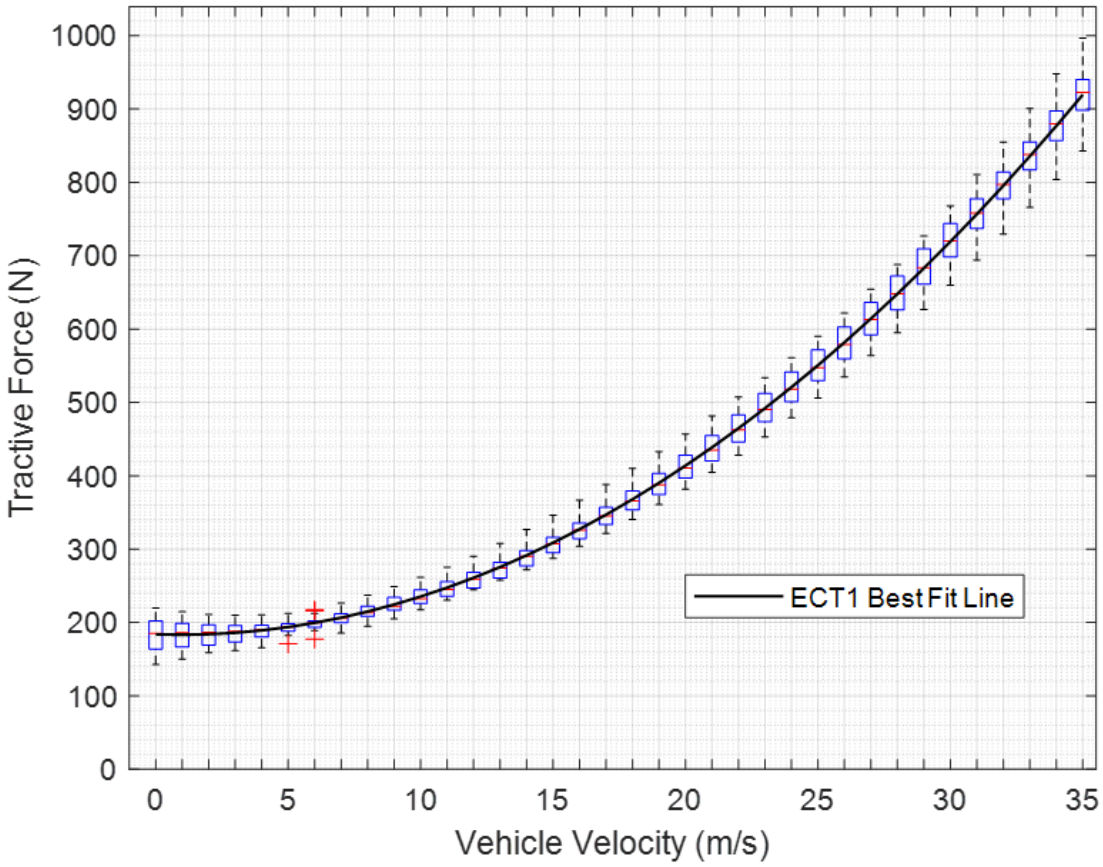

Figure 16: Box and Whisker Plot of the Calculated Tractive force from 0 to 35 m/s for the ECT1 coastdown condition with outliers removed

Visually, the results between the TCC condition and the ECT1 condition show little to no difference in both the overall tractive force trend as well as the values themselves. To fully understand the differences between the two control conditions, a further comparison was performed.

4.1.3 Control Conditions Comparison

In comparison to the TCC results, the ECT1 results demonstrate an overall lower range between the maximum and minimum values of tractive force at each vehicle speed. This range, at all vehicle velocities, is shown below in Figure 17. As this research pertains to an HEV it is important to mention that this discussion of range is for the statistic parameter of a data set's range and not the test vehicle's range. The standard deviations of each control condition at each vehicle velocity are also shown in Figure 17.

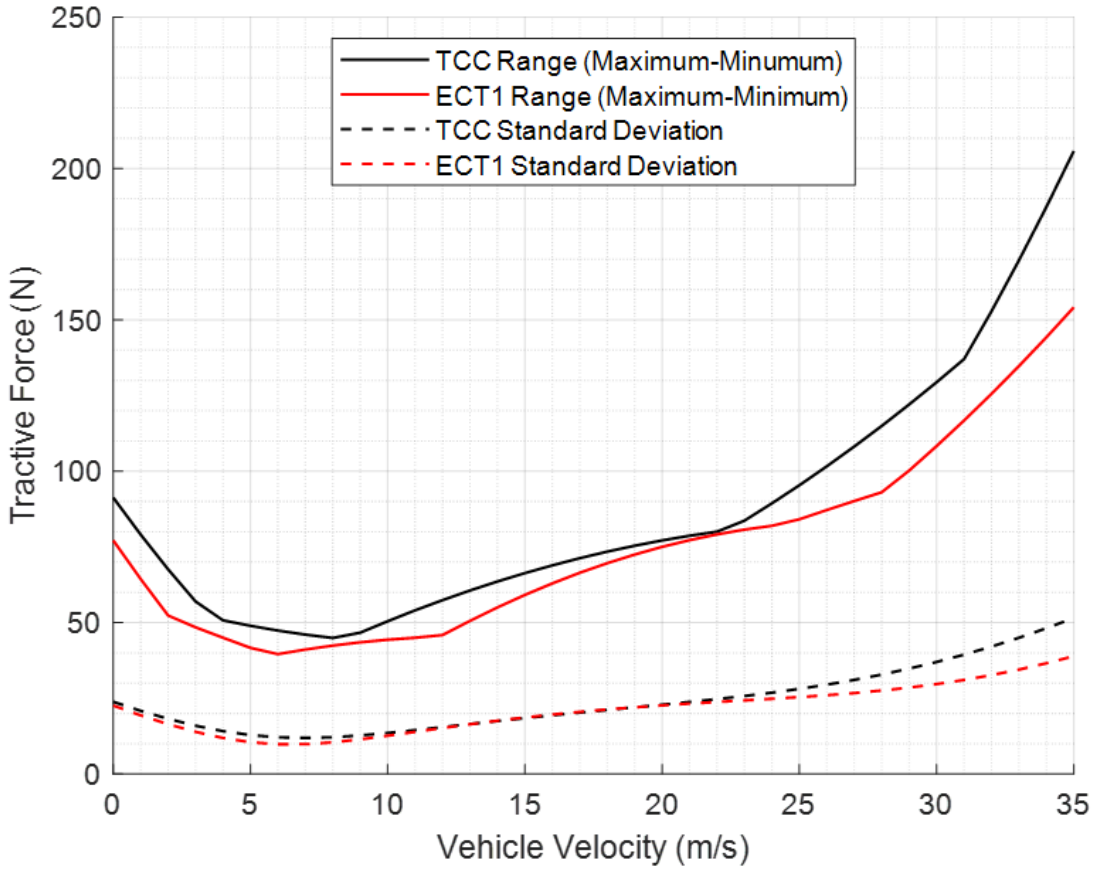

Figure 17: TCC and ECT1 range between maximum and minimum values and standard deviation of calculated tractive force at each vehicle velocity

The overall range differences in tractive force between the two control coastdown conditions are not substantially different enough except that the ECT1 condition has a lower range at all vehicle speeds. All this lower range does is improve justification for comparing the ECT2 and ECT3 coastdown conditions to the ECT1 as a control. Another justification for both conditions is the standard deviation curves. The standard deviation for both conditions is less than 30 N for the majority of vehicle speeds which is under half of the range. This would indicate that the majority of coastdown tests fall within one standard deviation of the mean and are viable for further analysis. The final comparison between the TCC and ECT1 conditions is to overlay the average tractive force at each vehicle speed for the ECT1 conditions with TCC's curve and box and whisker plot as shown below in Figure 18.

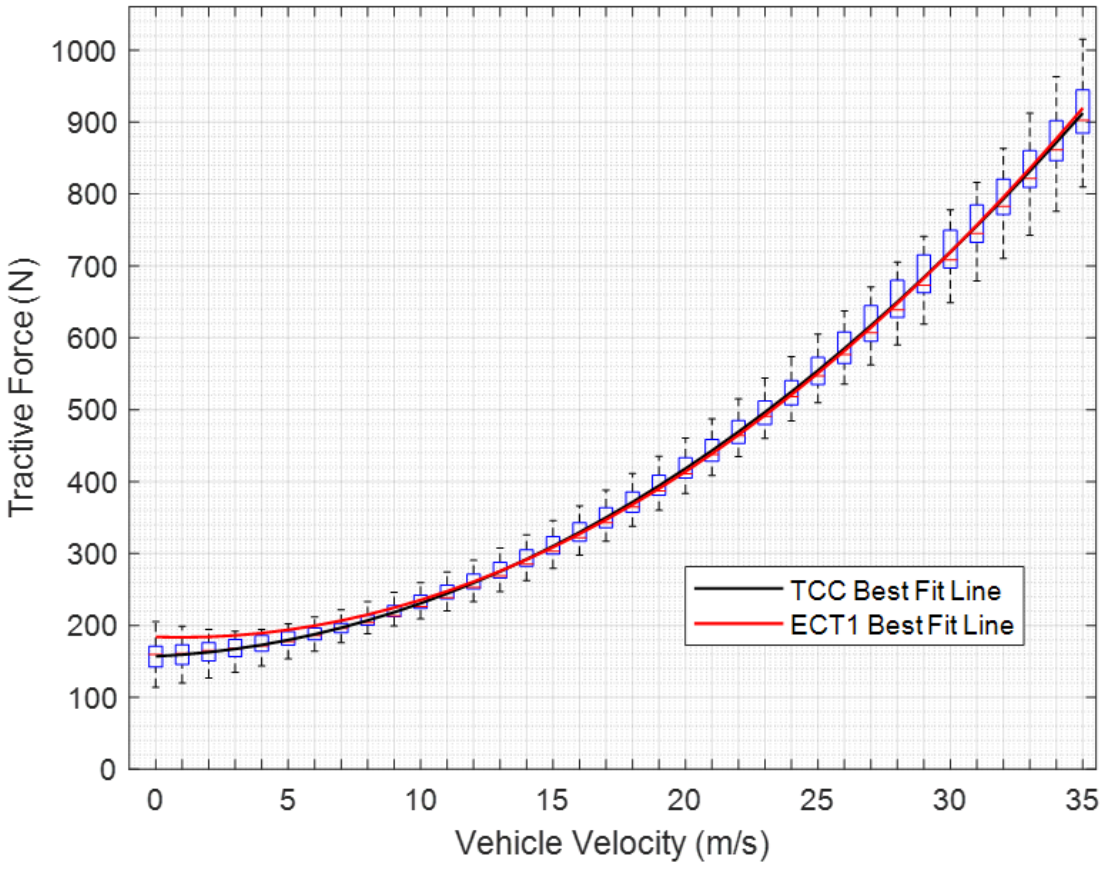

Figure 18: ECT1 best fit polynomial curve overlayed with the box and whisker plot from the TCC results

The overlay of the ECT1 best fit curve with the TCC box and whisker plot yields interesting results. It was expected that the results for the ECT1 test would display a higher tractive force due to the introduction of the internal rolling resistance of the EDU. However, the only region that indicates a noticeable difference in tractive force is below vehicle speeds of 5 m/s. In this region, the tractive force of the ECT1 coastdown condition is just on the edge of the upper quartile of the TCC results. To determine if there is a substantial statistical difference between the TCC and ECT1 results, the most noticeable difference in the comparison (vehicle velocity of 0 m/s) is explored a bit further in Table 7 below.

Table 7: Standard Deviation Comparison between TCC and ECT1 results at a Vehicle Velocity of 0 m/s

	TCC (N)	ECT1 (N)
Mean	157.11	183.93
Standard Deviation	23.86	22.61
1 Standard Deviation Higher	180.97	206.54
1 Standard Deviation Lower	133.25	161.32
Does the 1 standard deviation region overlap?	YES	

The standard deviation analysis indicates that the TCC and ECT1 results are not statistically different as their standard deviation regions overlap. However, the results from an unpaired *t* test dictate a P value of 0.0009 which indicates that the results are statistically significant. This means at a vehicle speed of 0 m/s, ECT1 is statistically different than TCC. The original assumption that the ECT1 tractive force would be higher than the TCC tractive force due to the addition of rolling resistance is a valid assumption at low vehicle speeds but not at high vehicle speeds. However, the analysis on the ECT2 and ECT3 results in comparison to the ECT1 results can still move forward as the ECT1 results are viable for full vehicle testing considering the "closeness" to TCC results.

4.2 Regenerative Braking Coastdown Results

The regenerative braking coastdown results are split between two different conditions. The only difference between the conditions are the value of the negative torque command to the EDU. The ECT2 condition features a smaller torque command where the ECT3 condition features a larger torque command. As mentioned previously, the magnitude of the command was determined through safety calibration with the test vehicle in the months prior to the full testing. As the regen torque commanded

is increased, the likely-hood of an oversteer event at high speeds increases due to the limitations of the rear tires' traction.

4.2.1 ECT2 Results

The ECT2 results are split between the two methodologies for determining and accounting for the back EMF forces from an engaged EDU. The first of the two methods is the measured torque method. Both methods will then be compared to the ECT1 results obtained previously to determine if the methods outlined by [25] are viable with a vehicle that can perform all methods. As a reminder, the ECT2 coastdown condition utilizes an engaged EDU clutch with a regenerative braking command of -200 Nm of torque to the EDU to replicate a vehicle that cannot be place into the proper configuration to follow a standard coastdown. For both methods, the resulting curves will be compared to the ECT1 results as they stand as the control for the engaged DU methodologies.

4.2.1.1 Measured Torque Method

The ECT2 test contains results for 17 coastdown tests. The reason that 18 coastdown tests are not analyzed is a battery SOC limit was reached during one of the coastdown tests causing a test abort at too high of a vehicle speed (~10 m/s). For this research, two methodologies were explored in accordance with [25] and Equations (4) and (5). The 17 coastdown tests (adjusted using the torque methodology defined in Equation (4)) are shown below in Figure 19. The polynomial curve fit coefficients for the average tractive force at each vehicle velocity are shown in Table 8.

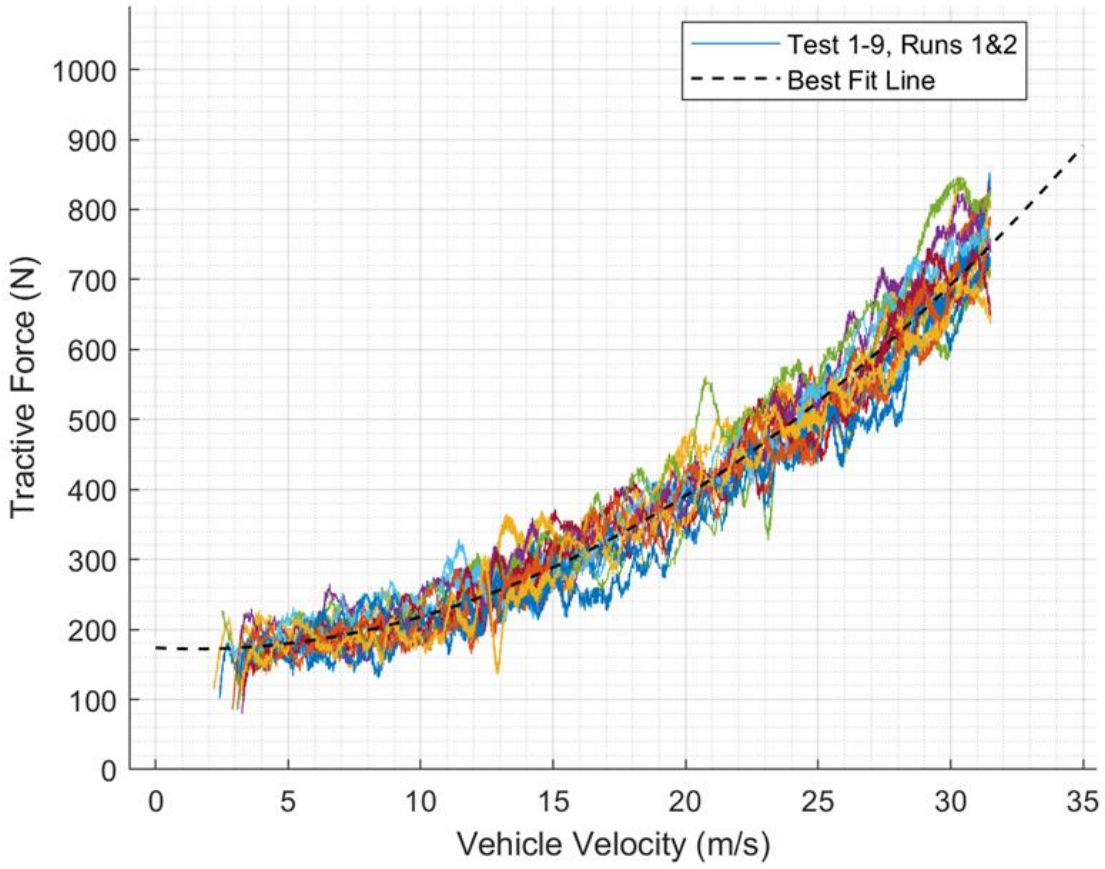

Figure 19: ECT2 results for the 17 coastdowns with the best fit line overlayed using the measured torque method to account for the back EMF forces

Table 8: ECT2 3-component road load constants 'A', 'B', and 'C' results from the 17 coastdowns using the measured torque method to account for the back EMF forces

A (N)	B $(\frac{N}{m/s})$	C $(\frac{N}{m^2/s^2})$
173.34	-1.973	0.636

The next step to analyze the measured torque ECT2 results follow the same methodology used for the ECT1 and TCC results. The box and whisker plot for the measured torque ECT2 results is shown below in Figure 20.

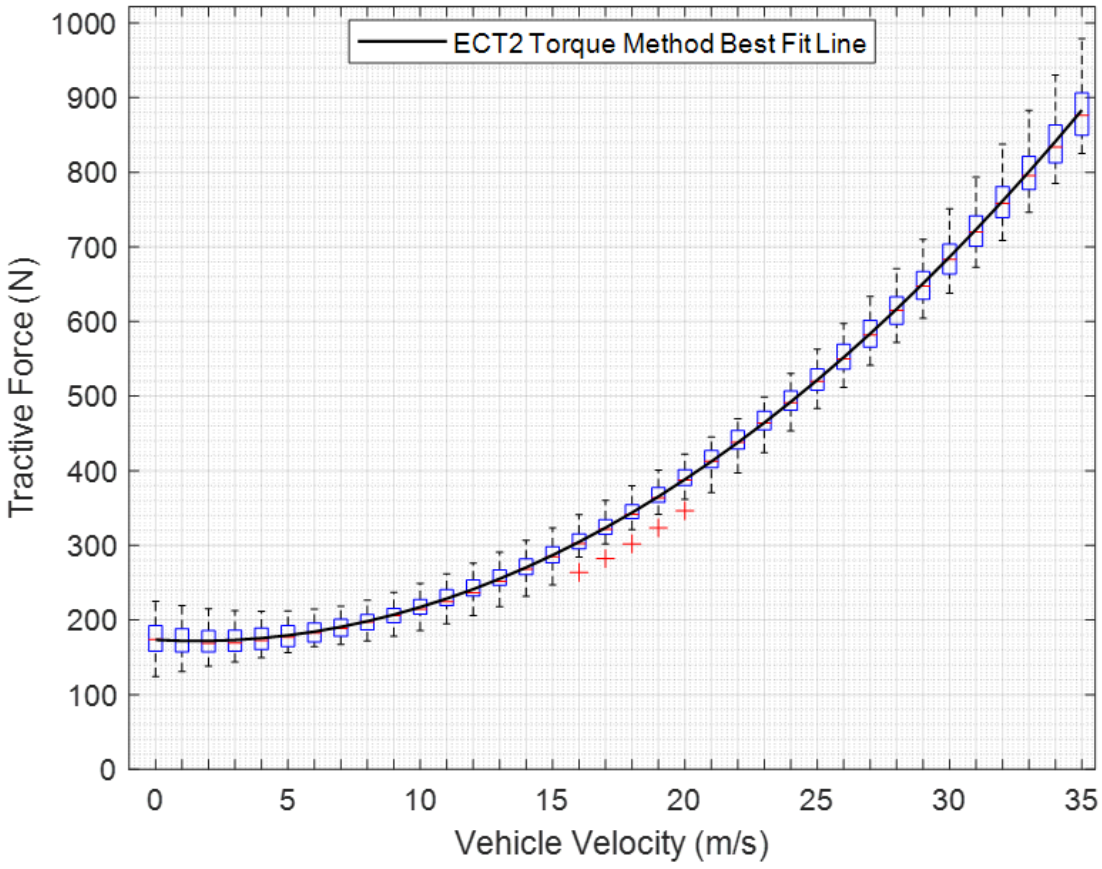

Figure 20: Box and Whisker Plot of the Calculated Tractive force from 0 to 35 m/s for the ECT2 measured torque method coastdown condition with outliers removed

An important observation with the ECT2 results is the increased spread in data and the increase in outliers present in the results. There 2 coastdowns that are considered outliers from the box and whisker creation. Only one of those outliers was removed from the data set due to excessively high tractive force between 27 and 35 m/s. This set was over 2.5 standard deviations and 2.11 interquartile ranges away from the median. That leaves 1 total outlier in Figure 20 for 16 coastdowns and it is considered in the results. The final comparison between the ECT2 results (for both methodologies) is shown in a later section.

4.2.1.2 Battery Power Method

The second methodology to account for the effects of an engaged EDU is using the battery power generated during a regenerative braking event to calculate (and account for) the back EMF forces. As defined in [25], this methodology is designed to be utilized by testers who do not have access to the test vehicle's torque signals but do have access to the vehicle's battery parameters. The set of coastdown data utilized for the battery powered method is the same 17 coastdowns used for the torque method. By standardizing the coastdowns used, it highlights the viability of the method without increasing test time required and increasing more variability into the results discussion. The 17 coastdowns along with the best fit polynomial curve are shown in Figure 21. The three terms of the polynomial curve fit are shown immediately following in Table 9.

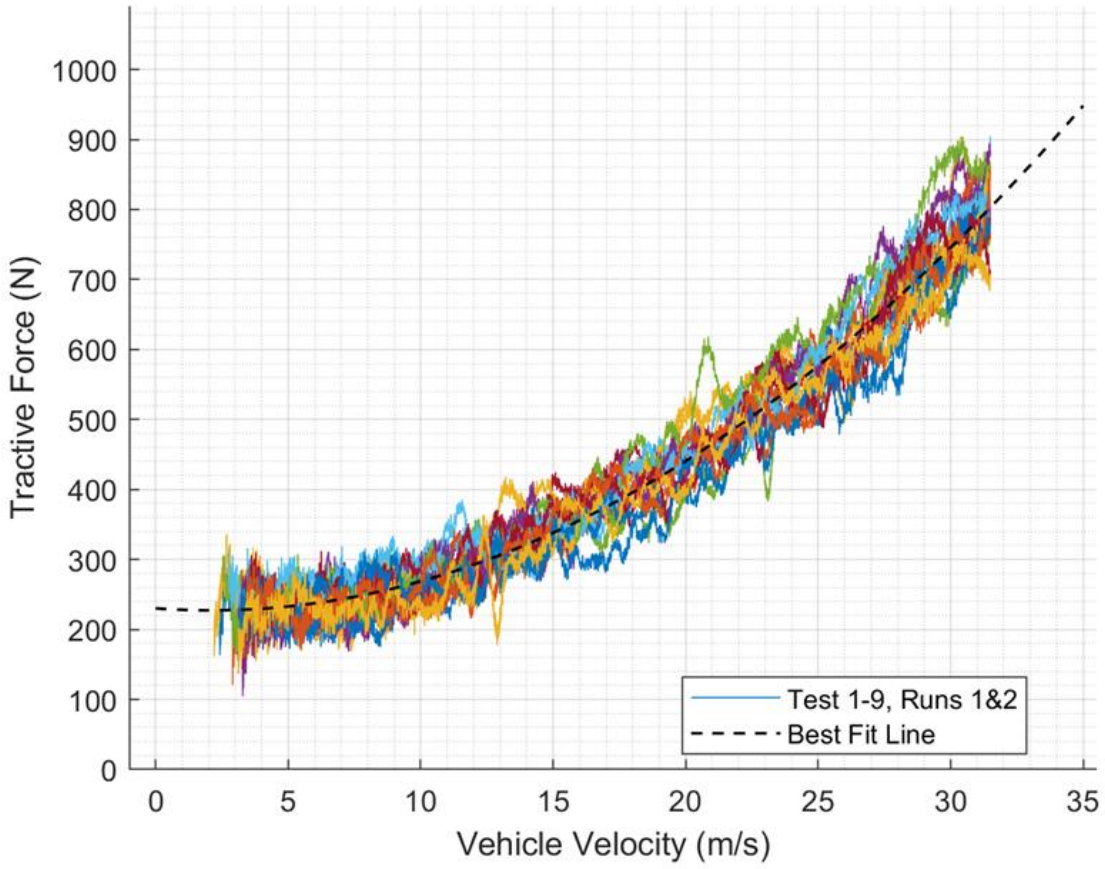

Figure 21: ECT2 results for the 17 coastdowns with the best fit line overlayed using the battery power method to account for the back EMF forces

Table 9: ECT2 3-component road load constants 'A', 'B', and 'C' results from the 17 coastdowns using the battery power method to account for the back EMF forces

A (N)	B $(\frac{N}{m/s})$	C $(\frac{N}{m^2/s^2})$
230.39	-2.835	0.661

The second term in the polynomial might signal alarm but the overall curve does not show any abnormalities in comparison to the general trend of the other coastdown conditions results. The same box and whisker plot methodology is utilized and shown below in Figure 22.

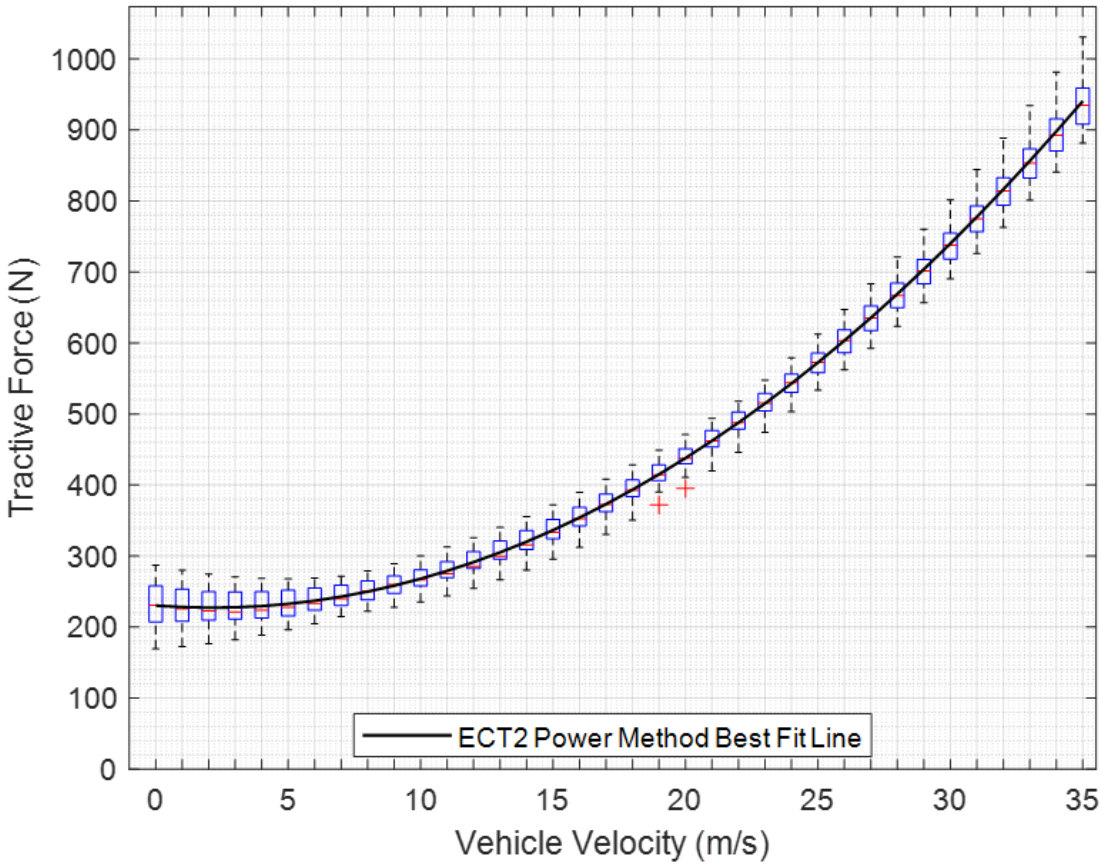

Figure 22: Box and Whisker Plot of the Calculated Tractive force from 0 to 35 m/s for the ECT2 battery power method coastdown condition with outliers removed

The same outlier removed from the torque methodology was also removed from the battery power methodology due to high tractive force at higher vehicle speeds and the differentiation from the median. This leaves 16 total coastdowns analyzed with a remaining 1 outlier using the battery power methodology for the ECT2 coastdown condition.

4.2.2 ECT2 Compared to ECT1 Results

With this research's ultimate goal of determining the viability of coastdown testing methods, the two methodologies discussed shall be compared to their control. The first step to understanding if there are

any substantial differences between the methodologies for ECT2 and ECT1 are to examine the range and standard deviation as shown in Figure 23 below.

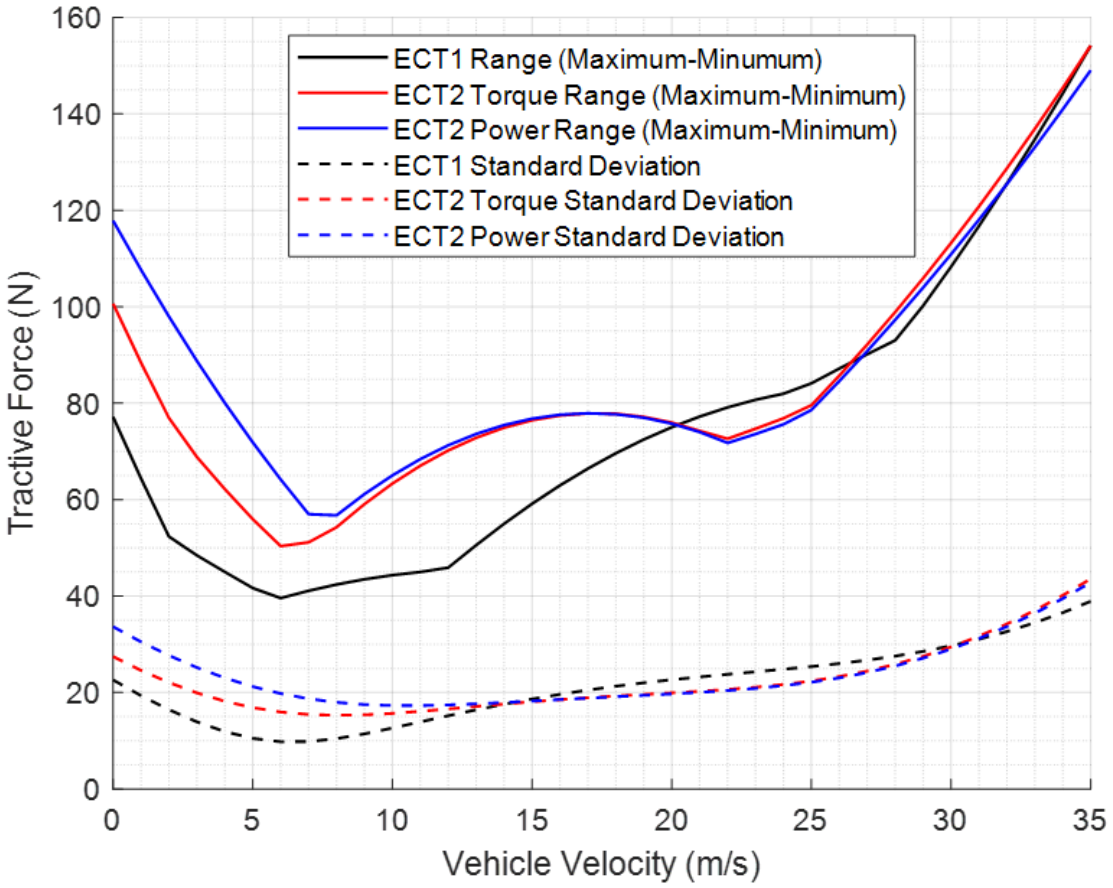

Figure 23: ECT1 and ECT2 (both methods) range between maximum and minimum values and standard deviation of calculated tractive force at each vehicle velocity

The two methodologies for the ECT2 have a considerably higher range of values for tractive force over the ECT1 results until 5 m/s. After this vehicle velocity, the ranges are similar. The standard deviation comparison between the ECT2 results and the ECT1 results show a similar trend as well which makes sense as the standard deviation is tied to the range of a data set. For further comparison, the two best fit polynomial curves for the ECT2 methodologies are overlayed with the ECT1 box and whisker results in Figure 24 below.

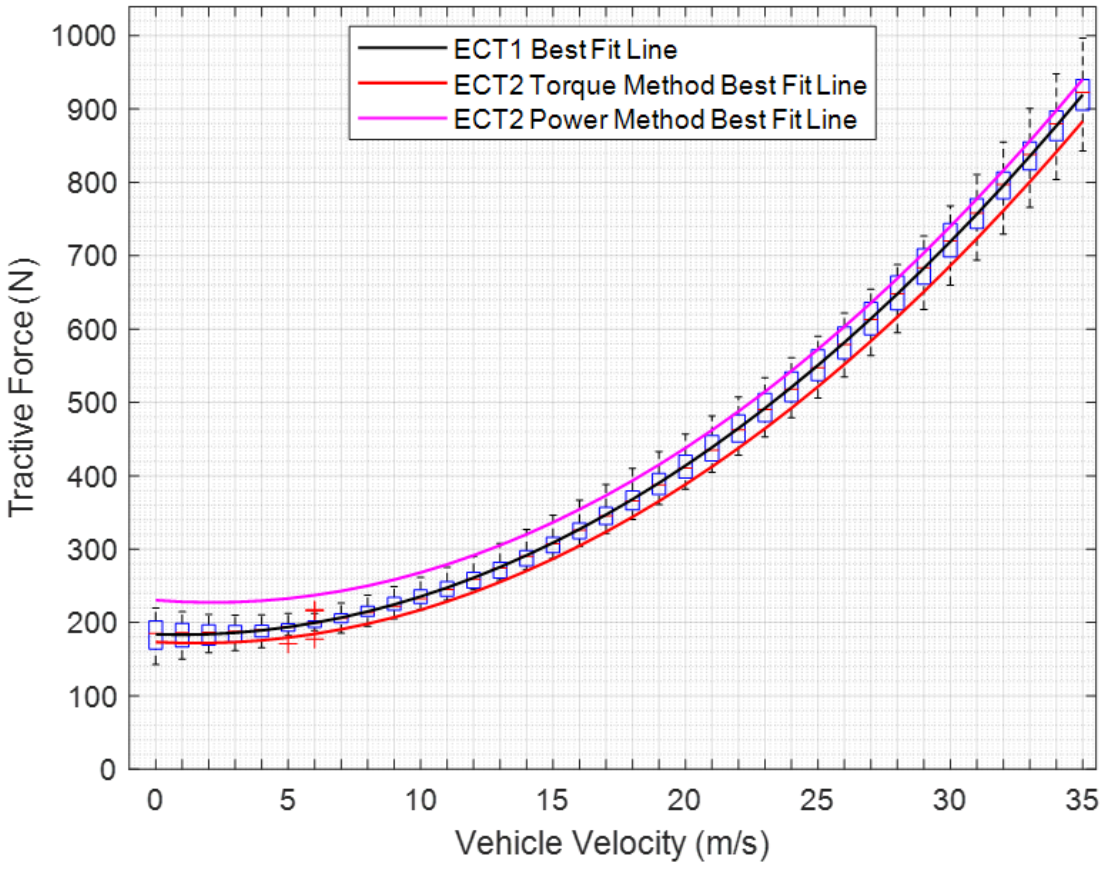

Figure 24: ECT2 best fit polynomial curves from both methods overlayed with the box and whisker plot from the ECT1 results

Overall, the curves themselves demonstrate very similar trends to the ECT1 results. The battery power method yielded a tractive force that is consistently higher than the control whereas the torque method yields consistently lower tractive force results over the same coastdowns. The battery power method fails to fall within the range of the ECT1 results below 8 m/s which is concerning when trying to justify this methodology to use in full vehicle testing. The torque method (while consistently lower) still stays within the range of the ECT1 results for the duration of the test. To determine if the curves demonstrate methodology viability with this testing vehicle, the ECT2 curves were then compared to the one standard deviation range of the ECT1 results as shown in Figure 25 below.

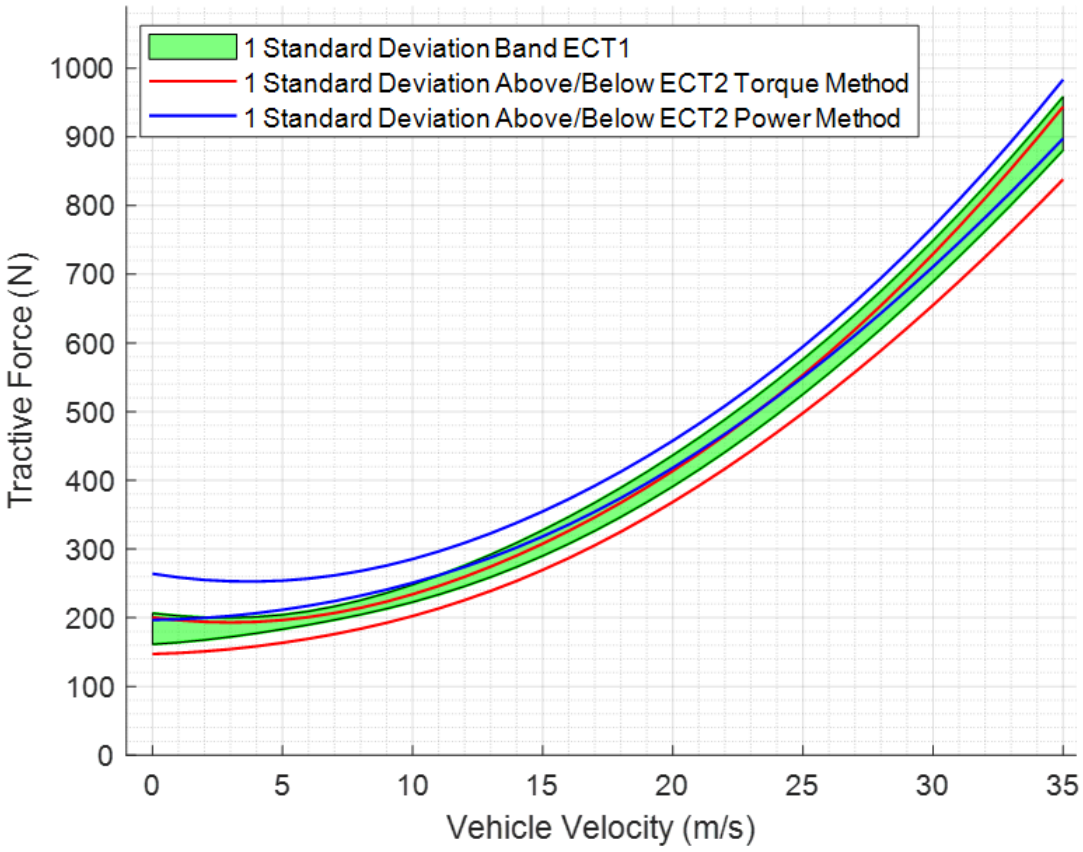

Figure 25: Comparison between ECT2 methods and the 1 standard deviation band for the ECT1 control

It is important to preface this discussion stating that both methodologies standard deviation bands intersect with the standard deviation band for ECT1 at almost all vehicle velocities. This means that only the torque method is truly viable at an EDU regen torque of -200 Nm. As the vehicle velocity decreases, the battery power method begins diverging more heavily from the ECT1 band and eventually leaves the one standard deviation band of ECT1 at 9 m/s. This will need to be monitored as the paper moves forward with the ECT3 results. The torque method follows the lower half of the band for one standard deviation from ECT1 for the full range of vehicle velocities. To be able to draw a full conclusion about the two methodologies, the ECT3 results must be analyzed. These results will show if the trends here are amplified or consistent at higher regen torque commands.

4.2.3 ECT3 Results

The ECT3 coastdown condition methodologies are the same as the ECT2 condition methodologies. The only difference in the two conditions is the amount of regen torque command. The ECT3 condition has a regen torque command of -400 Nm instead of -200 Nm. The two methodologies to analyze the 18 coastdown tests are the torque method and the battery power method.

4.2.3.1 Measured Torque Method

Unlike the ECT2 results, all 18 coastdown tests conducted will be analyzed as no battery SOC limits were reached and no other tests were aborted. If any outliers are present, they will be mentioned before analyzing the results. The 18 coastdown tests along with the resulting polynomial curve fit of the average tractive force at each vehicle velocity is below in Figure 26. The resulting coefficients of the curve fit are shown immediately following Figure 26 in Table 10.

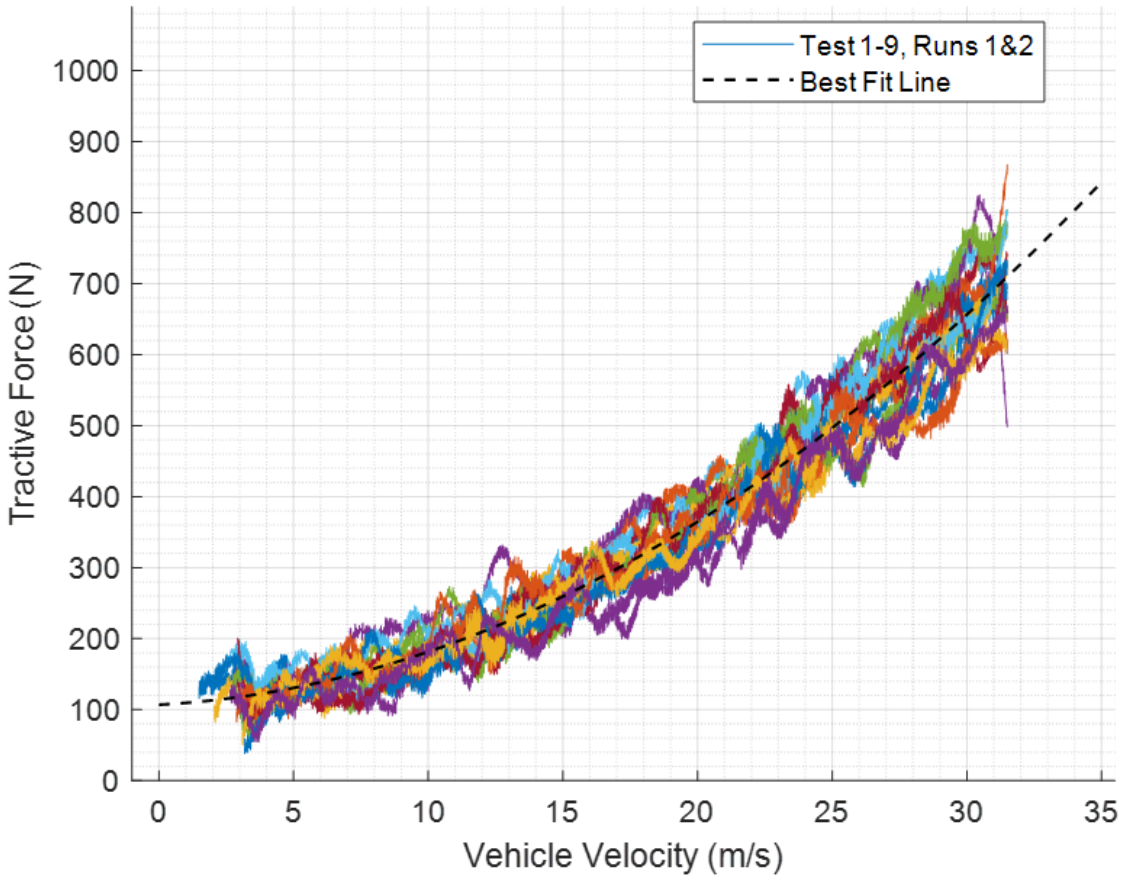

Figure 26: ECT3 results for the 18 coastdowns with the best fit line overlayed using the measured torque method to account for the back EMF forces

Table 10: ECT3 3-component road load constants 'A', 'B', and 'C' results from the 18 coastdowns using the measured torque method to account for the back EMF forces

A (N)	B $(\frac{N}{m/s})$	C $(\frac{N}{m^2/s^2})$
106.92	2.031	0.543

Right away, it is clear there are some differences between the ECT3 torque method and the ECT1 results. To start, the A term of the polynomial curve fit is much lower than the coefficient from the ECT1 results. This would indicate that the ECT3 torque method suggests the vehicle needs lower power to overcome the rolling resistance required to move than the ECT1 results. Considering ECT1 is the control

for this condition, this does not bode well for this test methodology comparison. The box and whisker plot for the ECT3 torque method along with the best fit line overlayed is shown below in Figure 27 to provide a better visual for the spread of tractive force at each vehicle velocity.

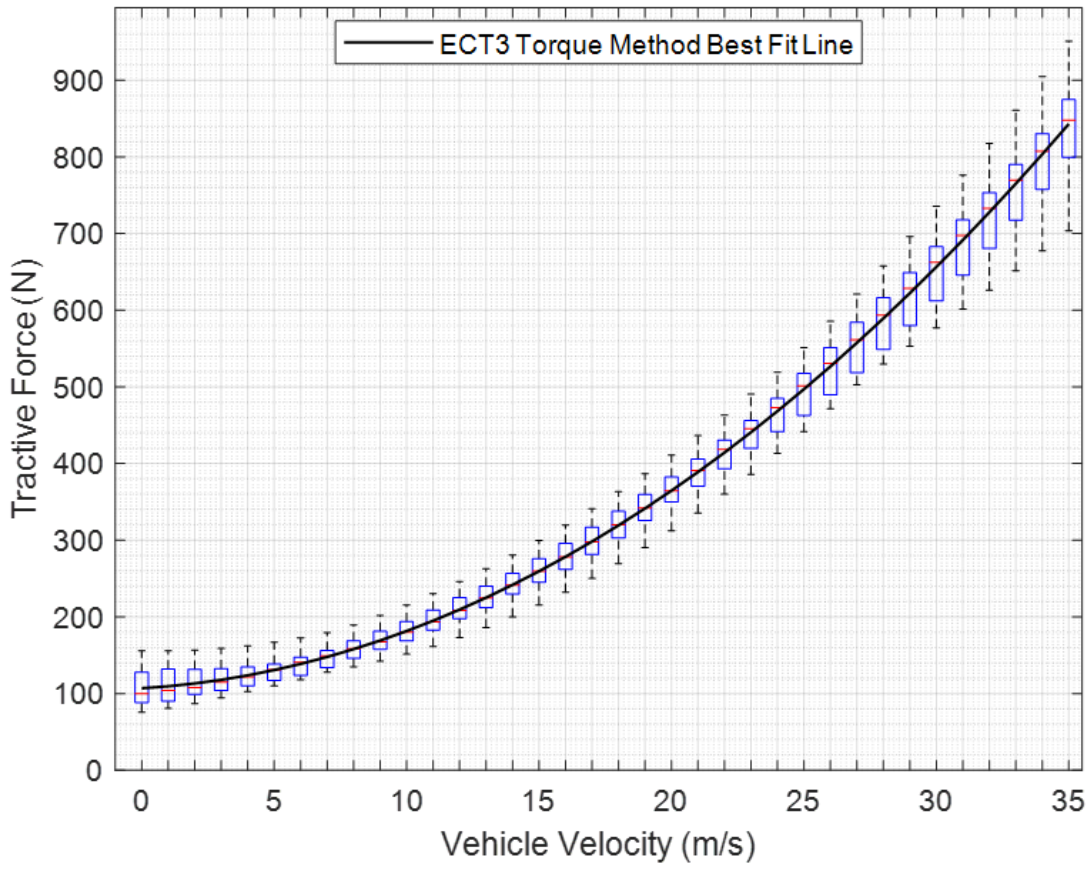

Figure 27: Box and Whisker Plot of the Calculated Tractive force from 0 to 35 m/s for the ECT3 measured torque method coastdown condition

For the measured torque method of ECT3, no outliers were present that needed removed from the data set to preserve the actual trend in the data. Even with no outliers present the range of tractive force at higher vehicle velocities is concerning. After documenting the battery power method for the ECT3 coastdown condition, the final comparison between ECT3 and the two methods to ECT1 will occur.

4.2.3.2 Battery Power Method

The ECT3 battery power method results for the 18 coastdowns along with the best fit polynomial curve and that curves coefficients are shown below in Figure 28 and Table 11.

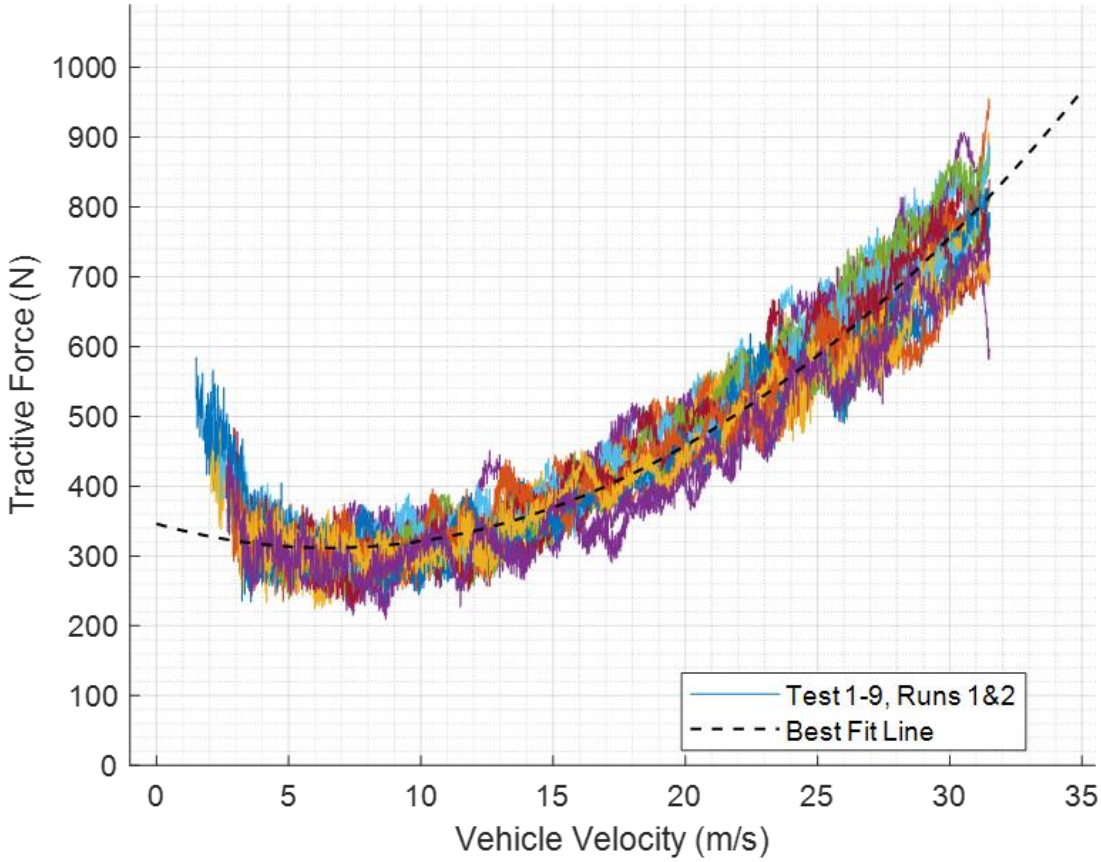

Figure 28: ECT3 results for the 18 coastdowns with the best fit line overlayed using the battery power method to account for the back EMF forces

Table 11: ECT3 3-component road load constants 'A', 'B', and 'C' results from the 18 coastdowns using the battery power method to account for the back EMF forces

A (N)	B $(\frac{N}{m/s})$	C $(\frac{N}{m^2/s^2})$
346.12	-10.56	0.808

In a sharp contrast to the measured toque method polynomial curve fit coefficients in Table 10, the coefficients for the battery power method indicate a much higher tractive force at low vehicle velocities. This follows the ECT2 results with a higher tractive force at low vehicle velocities but it is more exaggerated in comparison. As with all other results, the box and whisker plot of the data is shown below in Figure 29.

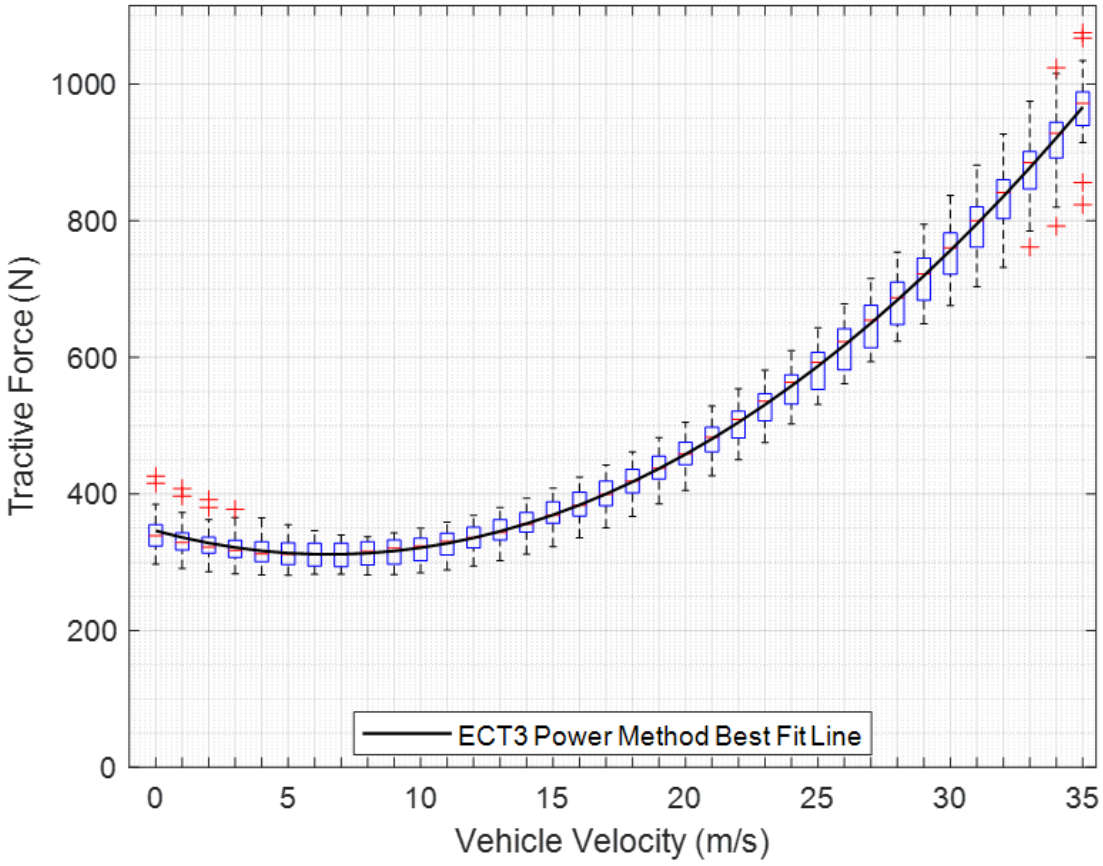

Figure 29: Box and Whisker Plot of the Calculated Tractive force from 0 to 35 m/s for the ECT3 battery power method coastdown condition

The outliers present at the low and high vehicle velocities were not removed as the expected trend of the tractive force was not violated. Another reason they were preserved is to keep the spirit of the research intact. If the results for the ECT3 torque method and the ECT3 power method had different

datasets due to outlier removal, the final conclusions would not have as much credibility as these results.

4.2.4 ECT3 Compared to ECT1 Results

To be able to draw a full conclusion about the viability of the sourced test methodology, a range of regenerative braking torques needed testing. The final comparison between the higher regen torque and the control is found here. As with the other two comparisons performed, the first step is to look at the tractive force's range and standard deviation at each vehicle velocity as shown in Figure 30.

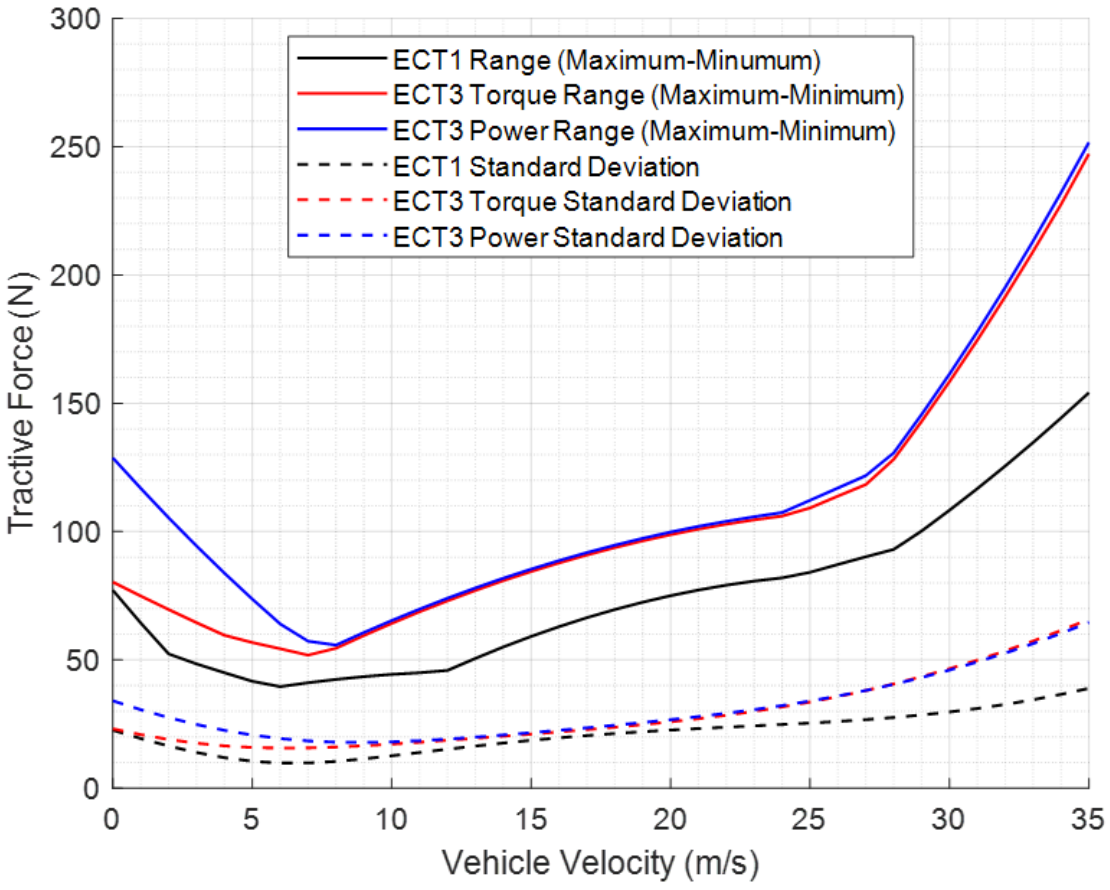

Figure 30: ECT1 and ECT3 (both methods) range between maximum and minimum values and standard deviation of calculated tractive force at each vehicle velocity

It is apparent right away that the range of the two ECT3 methods is higher than the control. However, from the standard deviation, the distribution is similar to the control. Unlike the ECT2 methods, the range does not improve a considerable amount with respect to the control. One thing that other visuals might highlight better is if the larger standard deviation of the ECT3 methodologies will negatively affect this conditions viability. Figure 31 below highlights how well the measured torque and battery power method for ECT3 fares against the ECT1 control's box and whisker plot.

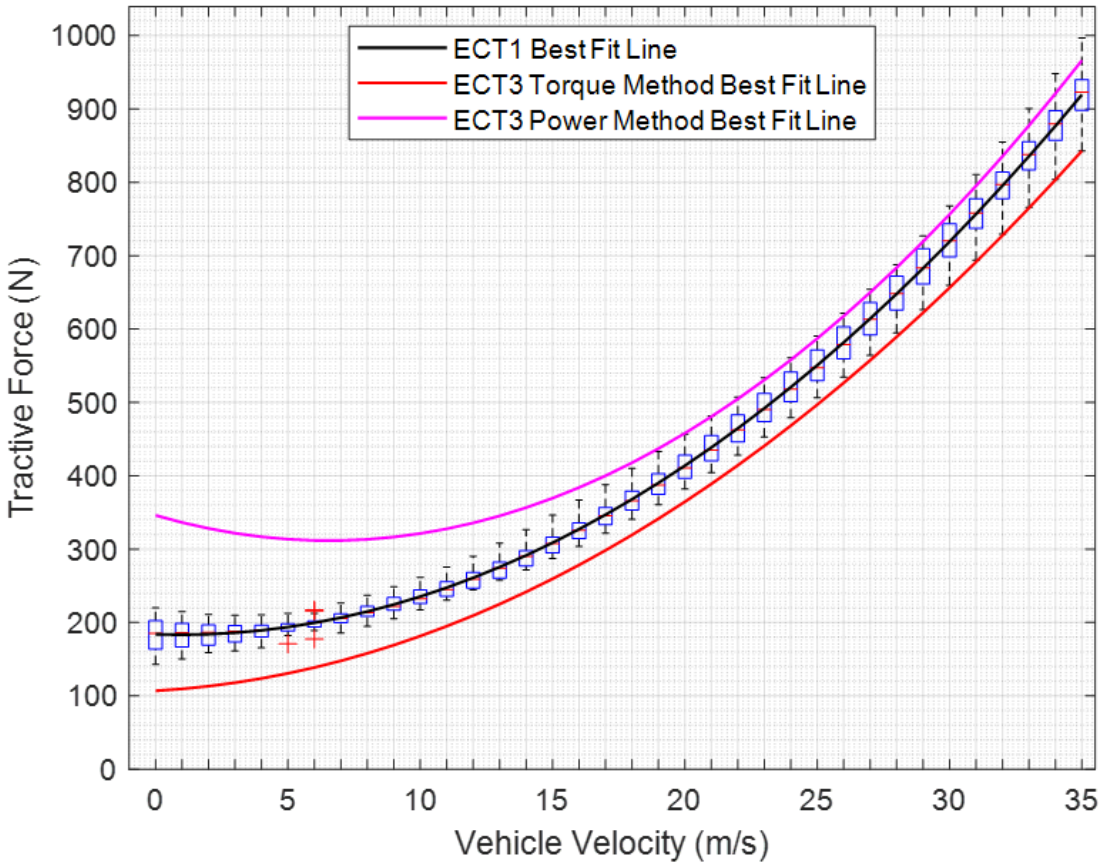

Figure 31: ECT3 best fit polynomial curves from both methods overlayed with the box and whisker plot from the ECT1 results

There is a clear difference between the ECT3 and the ECT2 results with respect to the best fit polynomials for the two methodologies. The battery power method has a more exaggerated upward trend at low vehicle velocities in comparison to the ECT2 results for the same methodology. The battery

power method stays within the range of ECT1 until a vehicle velocity of 17 m/s. The torque method for ECT3 also continues the trend of being lower than the ECT2 results. The torque method also fails to fall within the range of the ECT1 results for the entire vehicle velocity range. To see if either method is viable to use at this regen torque, the standard deviation bands for both ECT3 methods were compared to the ECT1 standard deviation band in Figure 32 below.

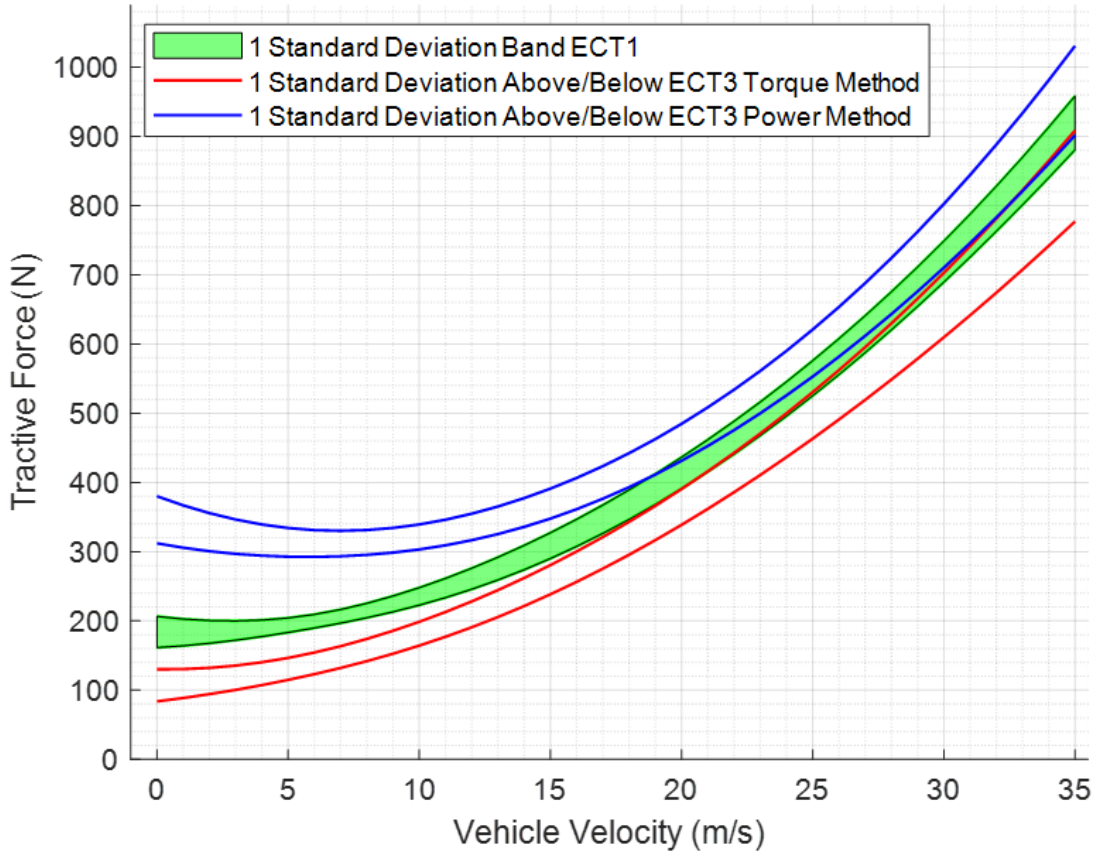

Figure 32: Comparison between ECT3 methods and the 1 standard deviation band for the ECT1 control

Both the battery power method and the measured torque method are not viable methodologies at a regen torque command of -400 Nm for all vehicle velocities below 15 m/s. The two methods' standard deviation bands overlap with the control's band for higher vehicle velocities indicating that the methods themselves are not completely incorrect for this specific vehicle. Out of the two methods, the measured

torque method follows the expected curve of the vehicle based on the ECT1 control better than the battery power method.

5. Conclusions and Recommendations

The overall goal of this work was to perform an established testing methodology for HEV and BEV that could not be placed into the proper configuration for a traditional coastdown. This means that it is imperative to account for the forces of the EDU in the tractive force calculation. This research explored two control coastdown conditions and two regenerative braking coastdown conditions. Throughout this exploration several key takeaways were found.

- When the EDU in this vehicle is engaged, it does not contain enough rolling resistance losses to be statistically different than when it is disconnected from the axle at high vehicle speeds. However, at 0 m/s the difference is significant, indicating that there are additional rolling resistance effects of the drive unit at low speeds.
- For this vehicle, the test methodologies used to account for back EMF forces using the torque method at a lower regenerative braking torque are within 1 standard deviation of the engaged EDU control.
- The methodologies used to account for back EMF forces are not adequate or viable for larger regenerative braking torque through the EDU. This could be for reasons addressed below in the fourth recommendation.
- The measured torque method to account for back EMF forces yields a tractive force that is consistently lower than the control but follows the same trend. With the higher regenerative braking torque command, this difference was also greater.
- The battery power method to account for the back EMF forces yields a tractive force that is closer to the control at higher vehicle velocities but begins to “hook” upwards as the vehicle velocity approaches 0 m/s. This upward “hook” increases with the higher regenerative braking

torque command possibly because of efficiency losses at high torque low speeds on the motor map.

- In vehicle testing at an outdoor test track yields a wide range of tractive forces providing larger range and standard deviations in the results.
- Logging timesteps in vehicle velocity require smoothing functions to generate acceleration vectors without discontinuities.
- Wind speed acting on the vehicle was approximated through two measurement methods and could account for higher range and standard deviation in the results.

The first recommendation for future work is to expand on the number of negative torque commands tested. This thesis explored two conditions with an engaged EDU provided a negative torque command. Ideally a future study would perform coastdowns over a wide array of negative torque commands to better define the trim and make a clear statement on when the commanded regen torque is too high for a vehicle. This exploration would provide a firmer conclusion about the initial trends found in this study.

The second recommendation for future work is to repeat this study on an AWD dynamometer. Many coastdown studies explored in this thesis expanded on their initial work by repeating coastdowns on a dynamometer. This repeat provides a more consistent and repeatable location to perform testing without the wind effects at a test track. As this research has already defined this vehicle's traditional road load coefficients from the TCC conditions, those parameters can be used to properly load the dynamometer before testing.

The third recommendation for future work is to expand the vehicle testing pool. If the testing pool was expanded to other vehicles, there is opportunity to explore the regenerative braking coastdown condition results with other types of vehicles. If the results are consistent with the results from this research then a broader conclusion about the testing methodology can be drawn.

The fourth and final recommendation is to expand upon the understanding of losses and contributions between the EDU and the battery. For the EDU, this research did not factor in the rotating inertia of the motor during the ECT1-3 testing. This rotating inertia creates an equivalent mass of the EDU which is not accounted for. This equivalent mass would have an effect to some degree on the lower speed road load versus velocity curves of this research. For the battery, inverter, and EDU, no electrical losses were factored into the results analysis. This could have an effect on the battery power methodology ECT2-3 results as they relied on the knowledge of the battery's voltage and current CAN messages. Without the addition of electrical losses between the HV components, there is an added degree of uncertainty to the results. The other uncertainty is how varied battery SOC effects the overall electrical losses.

References

[1] S. Cha, R. L. Sloan, and F. M. Black, “Study of Models for the Prediction of Average Road Load of In-Use Delivery Trucks,” 1983.

[2] “AVTC’s History – Advanced Vehicle Technology Competitions”, Accessed: Feb. 05, 2023. [Online]. Available: https://avtcseries.org/about-avtc/avtcs-history/

[3] M. Ehsani, Y. Gao, S. E. Gay, and A. Emadi, “Modern Electric, Hybrid Electric, and Fuel Cell Vehicles: Fundamentals, Theory, and Design,” 2005.

[4] Mathilde Carlier, “Gasoline-powered vehicles in the United States- statistics & facts,” 2021. [Online]. Available: https://www.statista.com/topics/4580/gasoline-powered-vehicles-in-the-united-states/#topicOverview2/6

[5] Michael Dwyer, “Electric vehicles and hybrids surpass 10% of U.S. light-duty vehicle sales,” Feb. 2022. [Online]. Available: https://www.eia.gov/todayinenergy/detail.php?id=51218

[6] “Emissions from Electric Vehicles.” [Online]. Available: https://energy.gov/eere/vehicles/technology-integration

[7] M. A. Miller, A. G. Holmes, B. M. Conlon, and P. J. Savagian, “The GM ‘Voltec’ 4ET50 Multi-Mode Electric Transaxle,” *SAE Int J Engines*, vol. 4, no. 1, pp. 2011-01–0887, Apr. 2011, doi: 10.4271/2011-01-0887.

[8] Idaho National Laboratory, “Vehicle Testing - Light Duty - BEV.” https://avt.inl.gov/vehicle-type/bev.html (accessed Feb. 06, 2023).

[9] A. R. Mull, “Powertrain Fuel Consumption Modeling and Benchmark Analysis Powertrain Fuel Consumption Modeling and Benchmark Analysis of a Parallel P4 Hybrid Electric Vehicle Using Dynamic of a Parallel P4 Hybrid Electric Vehicle Using Dynamic Programming Programming Recommended Citation Recommended Citation Mull, Aaron Robert, ‘Powertrain Fuel Consumption Modeling and Benchmark Analysis of a Parallel P4 Hybrid Electric Vehicle Using Dynamic Programming,’” 2021. [Online]. Available: https://researchrepository.wvu.edu/etd/10154

[10] J. A. Diethorn, “Implementation Of Fuzzy Logic Control Into An Equivalent Implementation Of Fuzzy Logic Control Into An Equivalent Minimization Strategy For Adaptive Energy Management Of A Minimization Strategy For Adaptive Energy Management Of A Parallel Hybrid Electric Vehicle Parallel Hybrid Electric Vehicle,” 2021. [Online]. Available: https://researchrepository.wvu.edu/etd

[11] J. Vincent, “What Is an EV Range Extender?,” *U.S. News Report*, Apr. 2022, Accessed: Feb. 08, 2023. [Online]. Available: https://cars.usnews.com/cars-trucks/advice/ev-range-extenders

[12] “HEV Types,” *Center for Advanced Automotive Technology*. http://autocaat.org/Technologies/Hybrid_and_Battery_Electric_Vehicles/HEV_Types/ (accessed Feb. 12, 2023).

[13] D. Lanzarotto, M. Marchesoni, M. Passalacqua, A. P. Prato, and M. Repetto, “Overview of different hybrid vehicle architectures,” Elsevier B.V., Jan. 2018, pp. 218–222. doi: 10.1016/j.ifacol.2018.07.036.

[14] M. De Santis, S. Agnelli, F. Patanè, O. Giannini, and G. Bella, “Experimental Study for the Assessment of the Measurement Uncertainty Associated with Electric Powertrain Efficiency Using the Back-to-Back Direct Method,” *Energies (Basel)*, vol. 11, no. 12, p. 3536, Dec. 2018, doi: 10.3390/en11123536.

[15] Argonne National Laboratory, “ECOCAR MOBILITY CHALLENGE,” 2022. https://avtcseries.org/about-avtc/past-competitions/ecocar-mobility-challenge/ (accessed Feb. 13, 2023).

[16] Argonne National Laboratory, “About the EcoCAR EV Challenge,” 2022. https://avtcseries.org/about-the-ecocar-ev-challenge/ (accessed Feb. 14, 2023).

[17] T. P. Harris, “Implementation of Radial Basis Function Artificial Neural Network Implementation of Radial Basis Function Artificial Neural Network into an Adaptive Equivalent Consumption Minimization Strategy into an Adaptive Equivalent Consumption Minimization Strategy for Optimized Control of a Hybrid Electric Vehicle for Optimized Control of a Hybrid Electric Vehicle,” 2020. [Online]. Available: https://researchrepository.wvu.edu/etd/7847

[18] Simona Onori, Lorenzo Serrao, and Giorgio Rizzoni, “Hybrid Electric Vehicles Energy Management Strategies,” Dec. 2016. doi: https://doi.org/10.1007/978-1-4471-6781-5.

[19] H. Son and H. Kim, “Development of Near Optimal Rule-Based Control for Plug-In Hybrid Electric Vehicles Taking into Account Drivetrain Component Losses,” *Energies (Basel)*, vol. 9, no. 6, p. 420, May 2016, doi: 10.3390/en9060420.

[20] T. A. Anderson, J. M. Barkman, and C. Mi, “Design and optimization of a fuzzy-rule based hybrid electric vehicle controller,” in *2008 IEEE Vehicle Power and Propulsion Conference*, IEEE, Sep. 2008, pp. 1–7. doi: 10.1109/VPPC.2008.4677545.

[21] Y. Shi, D. Reich, M. Epelman, E. Klampfl, and A. Cohn, “An analytical approach to prototype vehicle test scheduling,” *Omega (United Kingdom)*, vol. 67, pp. 168–176, Mar. 2017, doi: 10.1016/j.omega.2016.05.003.

[22] K. Tammi, T. Minav, and J. Kortelainen, “Thirty years of electro-hybrid powertrain simulation,” *IEEE Access*, vol. 6, pp. 35250–35259, Jun. 2018, doi: 10.1109/ACCESS.2018.2850916.

[23] MathWorks, “Virtual Vehicle Composer,” 2022. https://www.mathworks.com/help/vdynblks/ref/virtualvehiclecomposer-app.html (accessed Mar. 05, 2023).

[24] C. E. Chapin, “Road Load Measurement and Dynamometer Simulation Using Coastdown Techniques,” Jun. 1981. doi: 10.4271/810828.

[25] J. Wishart and J. Diez, “Test Specification-Coastdown Testing,” Phoenix, Nov. 2015.

[26] Argonne National Laboratory, “EcoCAR 3 - Advanced Vehicle Technology Competitions.” https://avtcseries.org/about-avtc/past-competitions/ecocar-3/ (accessed Feb. 25, 2023).

[27] S. Wayne and A. Nix, “Glider Model The Road Load Equation,” Morgantown, 2022.

[28] National Aeronautics and Space Administration, “The Drag Equation,” May 13, 2021. https://www.grc.nasa.gov/www/k-12/rocket/drageq.html#:~:text=The%20drag%20equation%20states%20that,times%20the%20reference%20area%20A. (accessed Feb. 27, 2023).

[29] H. Goodall and G. Thompson, “Prediction of Vehicle Reference Frontal Area,” *Technical Support Report for Regulatory Action*, Nov. 1977.

[30] J. W. Anderson, J. C. Firey, P. W. Ford, and W. C. Kieling, “Truck Drag Components by Road Test Measurement,” 1965.

[31] R. A. White and H. H. Korst, “The Determination of Vehicle Drag Contributions from Coast-Down Tests,” 1972. [Online]. Available: https://www.jstor.org/stable/44720684

[32] G. D. Thompson, “Prediction of Dynamometer Power Absorption to Simulate Light-Duty Vehicle Road Load,” Feb. 1977, doi: 10.4271/780617.

[33] T. P. Yasin, “The Analytical Basis of Automobile Coastdown Testing,” 1978. [Online]. Available: https://about.jstor.org/terms

[34] L. W. Deraad, “The Influence of Road Surface Texture on Tire Rolling Resistance,” Feb. 1978. doi: 10.4271/780257.

[35] B. A. P. Remenda, A. E. Krause, and P. Hertz, “Vehicle Coastdown Resistance Analysis Under Windy and Grade-Variable Conditions,” 1989. [Online]. Available: https://about.jstor.org/terms

[36] H. H. Korst and R. A. White, “Coastdown Tests: Determining Road Loads Versus Drag Component Evaluation,” 1990.

[37] F. T. Buckley, “ABCD - An Improved Coast Down Test and Analysis Method,” 1995.

[38] SAE, “20221017_SURFACE VEHICLE RECOMMENDED PRACTICE,” 1996.

[39] C. M. Crewe, M. A. Passmore, P. Symonds, and M. A. Passmore Loughborough Univ P Symonds, “Measurement of Formula One Car Drag Forces on the Test Track Measurement of Formula One Car Drag Forces on the Test Tra,” 1996.

[40] V. A. Petrushov, “Coast Down Method in Time-Distance Variables,” 1997.

[41] J. A. Walter, D. J. Pruess, and G. F. Romberg, “Coastdown/Wind Tunnel Drag Correlation and Uncertainty Analysis,” 2001.

[42] J. Howell, C. Sherwin, M. Passmore, and G. Le Good, “Aerodynamic Drag of a Compact SUV as Measured On-Road and in the Wind Tunnel,” 2002. [Online]. Available: https://www.jstor.org/stable/44719239

[43] W. Mayer and J. Wiedemann, “Road Load Determination Based on Driving-Torque-Measurement Driving-Torque-Measurement,” 2003.

[44] O. Heravi and M. Fogelberg, “Methodology to Predict Fuel Economy Benefits of Secondary Axle Disconnects on Four-Wheel-Drive / All-Wheel-Drive Vehicles,” 2005.

[45] Y. Meng, M. Jennings, P. Tsou, D. Brigham, D. Bell, and C. Soto, “Test Correlation Framework for Hybrid Electric Vehicle System Model,” *International Journal of Engines*, vol. 4, no. 1, pp. 1046–1057, 2011, doi: 10.2307/26278205.

[46] N. E. Ligterink, “Road load determination of passenger cars,” 2012. [Online]. Available: https://www.researchgate.net/publication/313248133

[47] R. “Barney” Carlson, H. Lohse-Busch, J. Diez, and J. Gibbs, “The Measured Impact of Vehicle Mass on Road Load Forces and Energy Consumption for a BEV, HEV, and ICE Vehicle,” *SAE International Journal of Alternative Powertrains*, vol. 2, no. 1, pp. 2013-01–1457, Apr. 2013, doi: 10.4271/2013-01-1457.

[48] L. G. Andersen and J. K. Larsen, “Introducing Functional Data Analysis to Coast Down Modeling for Rolling Resistance Estimation,” *SAE International Journal of Passenger Cars - Mechanical Systems*, vol. 8, no. 2, pp. 786–796, Jul. 2015, doi: 10.4271/2015-01-9111.

[49] C. Kim, H. Lee, Y. Park, C. L. Myung, and S. Park, “Study on the criteria for the determination of the road load correlation for automobiles and an analysis of key factors,” *Energies (Basel)*, vol. 9, no. 8, 2016, doi: 10.3390/en9080575.

[50] C. Paulina, D. Mcbryde, and M. Matthews, “Steady State Speeds Load Determinations Using Electric Vehicle Power or Dynamometer Measurements on Conventional Vehicles,” *Source: SAE International Journal of Engines*, vol. 10, no. 4, pp. 1820–1828, 2017, doi: 10.2307/26422569.

[51] A. Moskalik, “Using Transmission Data to Isolate Individual Losses in Coastdown Road Load Coefficients,” in *SAE Technical Papers*, SAE International, Apr. 2020. doi: 10.4271/2020-01-1064.

[52] Y. Singh, “Regression Models to Predict Coastdown Road Load for Various Vehicle Types,” The Ohio State University, Columbus, 2020.

[53] J. F. Shore, A. I. Christodoulias, A. S. Kolekar, F. E. Lockwood, and A. Kadiric, “Prediction of Electric Vehicle Transmission Efficiency Using a New Thermally Coupled Lubrication Model,” in *SAE Technical Papers*, SAE International, Apr. 2022. doi: 10.4271/2022-01-5026.

[54] L. D. V. Performance and E. M. Committee, “Road Load Measurement and Dynamometer Simulation Using Coastdown Techniques.” Mar. 2010. doi: https://doi.org/10.4271/J1263_201003.

[55] G. Beauregard and D. Karner, “ETA-HITP01 Revision 0 Effective ‘Road Load Measurement and Dynamometer Simulation Using Coast Down Techniques,’” Nov. 2004.

[56] “John Glen Columbus International Airport Weather Station,” *weatherunderground*. https://www.wunderground.com/history/daily/us/oh/columbus/KCMH/date/2023-4-29 (accessed May 10, 2023).

[57] MathWorks, “Help Center - blfread,” 2019. https://www.mathworks.com/help/vnt/ug/blfread.html (accessed May 08, 2023).

[58] MathWorks, “Help Center - sgolay,” 2006. https://www.mathworks.com/help/signal/ref/sgolay.html (accessed May 09, 2023).

[59] R. W. Schafer, “What is a savitzky-golay filter?,” *IEEE Signal Process Mag*, vol. 28, no. 4, pp. 111–117, 2011, doi: 10.1109/MSP.2011.941097.

[60] Y. Wang, Y. Zou, K. Henrickson, Y. Wang, J. Tang, and B.-J. Park, “Google Earth elevation data extraction and accuracy assessment for transportation applications,” *PLoS One*, vol. 12, no. 4, p. e0175756, Apr. 2017, doi: 10.1371/journal.pone.0175756.

[61] P. Zal, “Automobile Catalog.” https://www.automobile-catalog.com/auta_details1.php#gsc.tab=0 (accessed May 12, 2023).

[62] MathWorks, “Help Center - polyfit,” 2006. https://www.mathworks.com/help/matlab/ref/polyfit.html (accessed May 12, 2023).

[63] MathWorks, “Help Center - polyval,” 2006. https://www.mathworks.com/help/matlab/ref/polyval.html (accessed May 12, 2023).